# Reference-Based Dual Switch and Stay Diversity Systems Over Correlated Nakagami Fading Channels

Guillem Femenias, *Member, IEEE*

***Abstract*—In this paper, we provide new generic and exact analytical results for the performance of nonideal reference-based dual predetection switch and stay diversity systems in receiving $M$-ary digitally modulated signals in the presence of additive white Gaussian noise and correlated slow and nonselective Nakagami-$m$ fading channels. Pilot-tone-aided, pilot-symbol-aided, and differential detection (DD) reference-based systems are considered. The impact of symbol alphabet cardinality, normalized distance between antennas, fading severity, and normalized Doppler frequency on the performance of these systems is analyzed. Optimum switching threshold and optimum pilot-to-signal power ratio as a function of channel fading characteristics, normalized distance between antennas, and modulation type are determined. Furthermore, some fixed switching strategies—minimum cost strategy, fixed average strategy, and midpoint strategy—that allow one to obtain diversity gain with a reduced complexity receiver are considered.**

***Index Terms*—Correlated Nakagami fading, differential detection, pilot-symbol-aided systems, pilot-tone-aided systems, switched diversity.**

## I. Introduction

In the last several decades, considerable attention has been devoted to the study of adequate transmission techniques for wireless mobile communication systems. Based on the analysis of measurement data, the Nakagami distribution ($m$-distribution) [1], which was originally developed for fast fading processes in ionospheric and stratospheric propagation, has been found to be a fitting generalized model for the mobile radio channel [2]. Such a distribution can model different propagation conditions, providing more flexibility and higher accuracy in matching some experimental data than the commonly adopted Rayleigh, log-normal, and Rice distributions [2], [3]. Furthermore, the Nakagami model also has the advantage of including the Rayleigh distribution as a special case, and it can model fading conditions that are more or less severe than those of Rayleigh.

Space diversity reception, in which several signals received at different antennas are combined, is a well-known method that can be used to combat the effects of fading in wireless systems [4]. Over the years a variety of methods, such as *maximal ratio combining* (MRC), *equal gain combining* (EGC), or *selection combining* (SC), have evolved to capitalize on the uncorrelated fading exhibited by separate antennas in the space diversity array [5]. However, these combining methods require different amounts of knowledge of all the received signals in one form or another, and a dedicated communication receiver chain is needed for each diversity branch, which adds to the receiver complexity. A simpler though less efficient combining technique is switched-diversity reception [4]. In switched-diversity schemes, according to a specified switching strategy, only one branch is connected to the receiver at any time. Our analysis will be based on the discrete-time switching model described in [9]. Following a *switch and stay combining* (SSC) strategy, switching is produced only at discrete instants of time $t = nT$, where $n$ is an integer and $T$ is the interval between switching instants. Assuming a time-division multiple-access (TDMA) architecture, $T$ can be assumed to be the TDMA time slot duration. The switching is forced to occur during the dead time between time slots (a short time before each time-slot header used to avoid interference resulting from other ports because of small synchronization differences) [6]. In this way, the effects of the switching transients on the information symbols may be reduced or eliminated [6]. To assist with the demodulation process and channel state information (CSI) assessment, it is common practice to incorporate a reference signal (pilot symbols [8] or pilot tones [7]) alongside the transmitted data symbols. The use of reference-based systems allows the random FM noise and envelope fluctuations caused by multipath fading to be accurately tracked and eliminated, thus overcoming the error floor commonly associated with data transmission over fading channels.

It is the aim of this paper to derive the performance of a reference-based dual predetection switch and stay diversity system in receiving digitally modulated signals over correlated Nakagami fading channels. Previous work related to this topic can be found in [9]–[13] and references therein. Most of these papers limit their studies to the average error rate performance of binary differentially coherent and noncoherent schemes. In [12], Fedele analyzes the performance of $M$-ary differential phase-shift keying (MDPSK) schemes. In [13], Ko *et al.* provide analytical results for the performance of switch and stay combining schemes when used in conjunction with several $M$-ary signals that are candidates for high-rate transmission over fading channels. However, the general case of nonideal reference-based channel state information assessment and correlated signal strength fluctuations on the two diversity branches has not been yet investigated. Such a situation can be encountered, for example, in fast fading environments where the diversity antennas are closely spaced, with reference to the radio-frequency (RF) carrier wavelength, and then receive

Manuscript received July 29, 2001; revised November 28, 2002, February 20, 2003, and February 27, 2003. This work was supported in part by the Ministerio de Ciencia y Tecnologa and Fondo Europeo de Desarrollo Regional under Grant TIC2001-0287, Spain.

The author is with the Departament de Matemàtiques i Informàtica, Universitat de les Illes Balears, Balears 07011, Spain.

Digital Object Identifier 10.1109/TVT.2003.814217

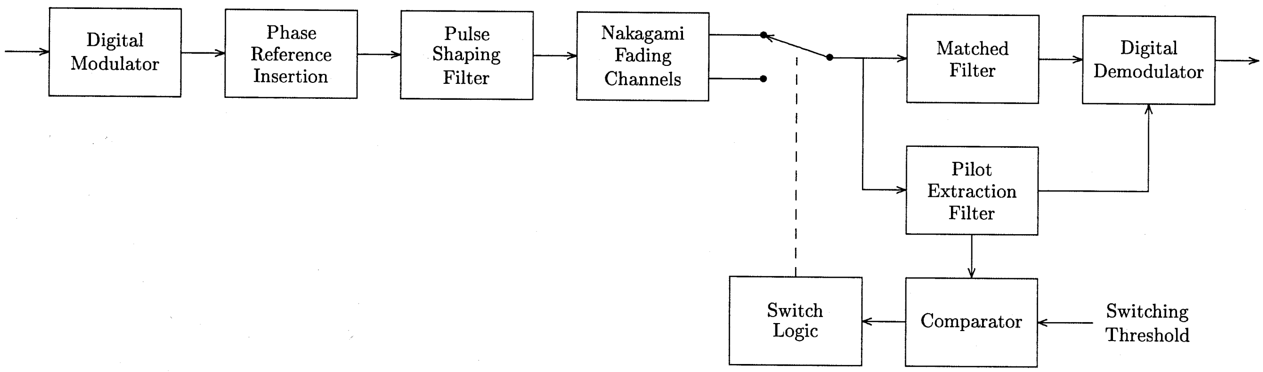


Fig. 1. Baseband system model.

fast signal fades pertaining to statistical distributions with a certain amount of correlation. In this paper, building on the analytical framework developed in [9]–[13], new generic and exact analytical results for the performance of nonideal reference-based dual predetection switch and stay diversity systems in receiving $M$-ary digitally modulated signals over correlated Nakagami fading channels are provided.

Since the performance of the reference-based switch and stay diversity system depends on the switching threshold and on the pilot-to-signal power ratio, it is possible to evaluate the values of these parameters that minimize the average symbol error rate. Thus, another goal of this paper is to determine the optimum switching threshold and the optimum pilot-to-signal power ratio as a function of modulation type, channel fading characteristics, normalized distance between antennas, and average signal-to-noise ratio (SNR). Furthermore, as the optimum adaptive switching threshold and the optimum pilot-to-signal power ratio could only be achieved by adapting them to the actual values of channel fading severity, average SNR at the matched filter and pilot extraction filter outputs, correlation coefficient between antennas, and correlation coefficient between matched filter output and pilot extraction filter output, then, in practical conditions, it can be appropriate to use fixed switching threshold and pilot-to-signal power ratio, which are independent of the actual values of system parameters. In order to set a fixed threshold and a fixed pilot-to-signal power ratio, based on the framework developed by Fedele in [12], fixed switching strategies—minimum cost strategy (MCS), fixed average strategy (FAS), and midpoint strategy (MPS)—that allow one to obtain diversity gain with a reduced complexity receiver are also considered.

The remainder of this paper is organized as follows. In Section II, the system model under consideration is briefly described and SSC output statistics, such as the cumulative distribution function (cdf), the probability density function (pdf), and the moment generating function (MGF), are derived. The general performance analysis in the case of reference-based reception of $M$-ary PSK signals by a dual switched-diversity combining system is provided in Section III. Adaptive and fixed switching threshold as well as pilot-to-signal power ratio optimization is also discussed in this section. The general results obtained in Section III are then applied to pilot-tone-aided systems (PTA), pilot-symbol-aided systems (PSA), and differential detection systems in Sections IV, V and VI, respectively. This paper is concluded in Section VII with a summary of the main results and contributions.

## II. System Model and SSC Output Statistics

The block diagram of the baseband system model under investigation is given in Fig. 1. A sequence of binary digits at rate $R_b = 1/T_b$ bits per second is modulated by an $M$-ary $(M = 2^k)$ digital modulator producing a sequence of symbols at rate $R_s = 1/T_s = 1/kT_b$ symbols per second. Following the modulation process, a phase reference signal is added to the data bearing signal. The composite signal is then pulse shaped and transmitted. The transmitted signal is faded and corrupted by additive white Gaussian noise passing through the Nakagami-$m$ fading channels. The received signal in the selected diversity branch is simultaneously passed to a matched filter and to a channel estimator. Finally, the data bearing signal is demodulated using the reference signal as CSI. The reference signal is also used to control the switching process.

Let $\gamma_{\text{ssc}}$, $\gamma_{\text{ssc}_\tau}$ and $\gamma_T$ denote the instantaneous SNR of the SSC pilot extraction filter output, the instantaneous SNR of the SSC matched filter output, and the predetermined switching threshold, respectively, and let $a_n$ denote a discrete-type random variable such as

$$a_n = \begin{cases} 1, & \text{if at } t = nT \text{ Rx connected to antenna 1} \\ 2, & \text{if at } t = nT \text{ Rx connected to antenna 2.} \end{cases} \quad (1)$$

In this case, following the mode of operation of SSC

$$a_n = \begin{cases} 1, & \text{iff} \begin{cases} a_{n-1} = 1 & \text{and } \gamma_{1,n} \geq \gamma_T \\ & \text{or} \\ a_{n-1} = 2 & \text{and } \gamma_{2,n} < \gamma_T \end{cases} \\ 2, & \text{iff} \begin{cases} a_{n-1} = 2 & \text{and } \gamma_{2,n} \geq \gamma_T \\ & \text{or} \\ a_{n-1} = 1 & \text{and } \gamma_{1,n} < \gamma_T \end{cases} \end{cases} \quad (2)$$

$$\gamma_{\text{ssc}} = \begin{cases} \gamma_{1,n}, & \text{if } a_n = 1 \\ \gamma_{2,n}, & \text{if } a_n = 2 \end{cases} \quad (3)$$

$$\gamma_{\text{ssc}_\tau} = \begin{cases} \gamma_{1\tau,n}, & \text{if } a_n = 1 \\ \gamma_{2\tau,n} & \text{if } a_n = 2 \end{cases} \quad (4)$$

where $\gamma_{i,n}$ and $\gamma_{i\tau,n}$ denote the instantaneous SNRs of the SSC pilot extraction filter output and the SSC matched filter output, respectively, if at $t = nT^{-}$ the receiver is connected to the $i$th antenna. Thus, the cdf of $\gamma_{\mathrm{ssc}_\tau}$ can be written as

$$\begin{aligned} P_{\gamma_{\mathrm{ssc}_\tau}}(\gamma) &\triangleq Pr\{\gamma_{\mathrm{ssc}_\tau} \le \gamma\} \\ &= Pr\{\gamma_{\mathrm{ssc}_\tau} \le \gamma | a_n = 1\} Pr\{a_n = 1\} \\ &\quad + Pr\{\gamma_{\mathrm{ssc}_\tau} \le \gamma | a_n = 2\} Pr\{a_n = 2\} \\ &= Pr\{\gamma_{1\tau,n} \le \gamma \text{ and } a_n = 1\} \\ &\quad + Pr\{\gamma_{2\tau,n} \le \gamma \text{ and } a_n = 2\}. \end{aligned} \tag{5}$$

Using (2) in (5), we have

$$\begin{aligned} &P_{\gamma_{\mathrm{ssc}_\tau}}(\gamma) \\ &\triangleq Pr\{a_{n-1} = 1 \text{ and } \gamma_{1,n} \ge \gamma_T \text{ and } \gamma_{1\tau,n} \le \gamma\} \\ &\quad + Pr\{a_{n-1} = 2 \text{ and } \gamma_{2,n} < \gamma_T \text{ and } \gamma_{1\tau,n} \le \gamma\} \\ &\quad + Pr\{a_{n-1} = 2 \text{ and } \gamma_{2,n} \ge \gamma_T \text{ and } \gamma_{2\tau,n} \le \gamma\} \\ &\quad + Pr\{a_{n-1} = \text{ and } \gamma_{1,n} < \gamma_T \text{ and } \gamma_{2\tau,n} \le \gamma\}. \end{aligned} \tag{6}$$

Assuming that the interval between switching instants is large enough in order that we can consider independency between the events at $\mathrm{t} = \mathrm{nT}$ and $\mathrm{t} = (\mathrm{n}-1)\mathrm{T}$ and using the fact that the events $a_n = 1$ and $a_n = 2$ are mutually exclusive, then we can rewrite (6) as

$$\begin{aligned} P_{\gamma_{\mathrm{ssc}_\tau}}(\gamma) &= p_1(\gamma_T)\,[Pr\{\gamma_{1,n} \ge \gamma_T \text{ and } \gamma_{1\tau,n} \le \gamma\} \\ &\qquad + Pr\{\gamma_{1,n} < \gamma_T \text{ and } \gamma_{2\tau,n} \le \gamma\}] \\ &\quad + p_2(\gamma_T)\,[Pr\{\gamma_{2,n} \ge \gamma_T \text{ and } \gamma_{2\tau,n} \le \gamma\} \\ &\qquad + Pr\{\gamma_{2,n} < \gamma_T \text{ and } \gamma_{1\tau,n} \le \gamma\}] \\ &= p_1(\gamma_T)\,[Pr\{\gamma_{1\tau,n} \le \gamma\} \\ &\qquad - Pr\{\gamma_{1,n} < \gamma_T \text{ and } \gamma_{1\tau,n} \le \gamma\} \\ &\qquad + Pr\{\gamma_{1,n} < \gamma_T \text{ and } \gamma_{2\tau,n} \le \gamma\}] \\ &\quad + p_2(\gamma_T)\,[Pr\{\gamma_{2\tau,n} \le \gamma\} \\ &\qquad - Pr\{\gamma_{2,n} < \gamma_T \text{ and } \gamma_{2\tau,n} \le \gamma\} \\ &\qquad + Pr\{\gamma_{2,n} < \gamma_T \text{ and } \gamma_{1\tau,n} \le \gamma\}] \end{aligned} \tag{7}$$

with [13, (59)–(61)]

$$\begin{aligned} p_1(\gamma_T) &\triangleq Pr\{a_{n-1} = 1\} = \frac{P_{\gamma_2}(\gamma_T)}{P_{\gamma_1}(\gamma_T) + P_{\gamma_2}(\gamma_T)} \\ &= \frac{\Gamma(m) - \Gamma\left(m, \frac{m}{\overline{\gamma}_2}\gamma_T\right)}{2\Gamma(m) - \Gamma\left(m, \frac{m}{\overline{\gamma}_1}\gamma_T\right) - \Gamma\left(m, \frac{m}{\overline{\gamma}_2}\gamma_T\right)} \\ p_2(\gamma_T) &\triangleq Pr\{a_{n-1} = 2\} = \frac{P_{\gamma_1}(\gamma_T)}{P_{\gamma_1}(\gamma_T) + P_{\gamma_2}(\gamma_T)} \\ &= \frac{\Gamma(m) - \Gamma\left(m, \frac{m}{\overline{\gamma}_1}\gamma_T\right)}{2\Gamma(m) - \Gamma\left(m, \frac{m}{\overline{\gamma}_1}\gamma_T\right) - \Gamma\left(m, \frac{m}{\overline{\gamma}_2}\gamma_T\right)} \end{aligned} \tag{8}$$

where $P_\gamma(\cdot)$ represents the cdf of $\gamma$, $m$ is the Nakagami fading parameter [1], $\Gamma(\cdot)$ is the gamma function, and $\Gamma(\cdot,\cdot)$ is the complementary incomplete gamma function. Substituting (8) in (7), the cdf of $\gamma_{\mathrm{ssc}_\tau}$ can be expressed solely in terms of the joint and marginal cdfs of the random variables $\gamma_{1,n}$, $\gamma_{2,n}$, $\gamma_{1\tau,n}$, and $\gamma_{2\tau,n}$ as

$$\begin{aligned} P_{\gamma_{\mathrm{ssc}\tau}}(\gamma) &= p_1(\gamma_T)\,[P_{\gamma_{1\tau}}(\gamma) - P_{\gamma_1,\gamma_{1\tau}}(\gamma_T,\gamma) \\ &\qquad + P_{\gamma_1,\gamma_{2\tau}}(\gamma_T,\gamma)] \\ &\quad + p_2(\gamma_T)\,[P_{\gamma_{2\tau}}(\gamma) - P_{\gamma_2,\gamma_{2\tau}}(\gamma_T,\gamma) \\ &\qquad + P_{\gamma_2,\gamma_{1\tau}}(\gamma_T,\gamma)]\,. \end{aligned} \tag{9}$$

Differentiating $P_{\gamma_{\mathrm{ssc}_\tau}}(\gamma)$ as given by (9) with respect to $\gamma$, we get the pdf of $\gamma_{\mathrm{ssc}_\tau}$ as

$$\begin{aligned} P_{\gamma_{ssc_\tau}}(\gamma) &= p_1(\gamma_T)\left[P_{\gamma_{1\tau}}(\gamma) - \int_0^{\gamma_T} P_{\gamma_1,\gamma_{1\tau}}(x,\gamma)dx \right. \\ &\qquad \left. + \int_0^{\gamma_T} P_{\gamma_1,\gamma_{2\tau}}(x,\gamma)dx\right] \\ &\quad + p_2(\gamma_T)\left[P_{\gamma_{2\tau}}(\gamma) - \int_0^{\gamma_T} P_{\gamma_2,\gamma_{2\tau}}(x,\gamma)dx \right. \\ &\qquad \left. + \int_0^{\gamma_T} P_{\gamma_2,\gamma_{1\tau}}(x,\gamma)dx\right] \end{aligned} \tag{10}$$

or, equivalently

$$\begin{aligned} p_{\gamma_{\mathrm{ssc}_\tau}}(\gamma) &= p_1(\gamma_T)\left[p_{\gamma_{1\tau}}(\gamma) + \int_{\gamma_T}^{\infty} p_{\gamma_1,\gamma_{1\tau}}(x,\gamma)dx \right. \\ &\qquad \left. - \int_{\gamma_T}^{\infty} p_{\gamma_1,\gamma_{2\tau}}(x,\gamma)dx\right] \\ &\quad + p_2(\gamma_T)\left[p_{\gamma_{2\tau}}(\gamma) + \int_{\gamma_T}^{\infty} p_{\gamma_2,\gamma_{2\tau}}(x,\gamma)dx \right. \\ &\qquad \left. - \int_{\gamma_T}^{\infty} p_{\gamma_2,\gamma_{1\tau}}(x,\gamma)dx\right]. \end{aligned} \tag{11}$$

In the case of correlated Nakagami-$m$ fading envelopes, the joint pdf $p_{R_i,R_j}(R_i,R_j)$ of $R_i \triangleq \sqrt{\gamma_i}$ and $R_j \triangleq \sqrt{\gamma_j}$ is given by [1, (126)]

$$\begin{aligned} p_{R_i,R_j}(R_i,R_j) &= \frac{4m^{m+1} R_i^m R_j^m e^{\frac{-m\left(R_i^2\overline{\gamma}_2 + R_j^2\overline{\gamma}_i\right)}{\overline{\gamma}_i\overline{\gamma}_j(1-\rho_{i,j})}}}{(\overline{\gamma}_i\overline{\gamma}_j)^{\frac{(m+1)}{2}}\Gamma(m)\rho_{i,j}^{\frac{(m-1)}{2}}(1-\rho_{i,j})} \\ &\quad \times I_{m-1}\left(\frac{2m\sqrt{\rho_{i,j}}R_iR_j}{(\overline{\gamma}_i\overline{\gamma}_j)^{\frac{1}{2}}(1-\rho_{i,j})}\right), \\ &\quad R_i \ge 0,\ R_j \ge 0 \end{aligned} \tag{12}$$

where $\rho_{i,j}$ is the correlation coefficient between $\gamma_i$ and $\gamma_j$, and $I_n(\cdot)$ denotes the modified Bessel function of order $n$. Using [15, p. 143], the joint pdf of $\gamma_i$ and $\gamma_j$ can be written as

$$\begin{aligned} p_{\gamma_i,\gamma_j}(\gamma_i,\gamma_j) &= \frac{m^{m+1}\gamma_i^{\frac{(m-1)}{2}}\gamma_j^{\frac{(m-1)}{2}} e^{\frac{-m(\gamma_i\overline{\gamma}_j + \gamma_j\overline{\gamma}_i)}{\overline{\gamma}_i\overline{\gamma}_j(1-\rho_{i,j})}}}{(\overline{\gamma}_i\overline{\gamma}_j)^{\frac{(m+1)}{2}}\Gamma(m)\rho_{i,j}^{\frac{(m-1)}{2}}(1-\rho_{i,j})} \\ &\quad \times I_{m-1}\left(\frac{2m\sqrt{\rho_{i,j}\gamma_i\gamma_j}}{(\overline{\gamma}_i\overline{\gamma}_j)^{\frac{1}{2}}(1-\rho_{i,j})}\right), \\ &\quad \gamma_i \ge 0,\ \gamma_j \ge 0. \end{aligned} \tag{13}$$

Thus, using [16, (7)], the integral terms of (11) can be expressed as a function of the $m$th order Marcum $Q$-function as

$$\begin{aligned}\omega_{i,j}(\gamma) &\triangleq \int_{\gamma_T}^{\infty} p_{\gamma_i,\gamma_j}(x,\gamma)dx \\ &= \frac{\left(\frac{m}{\overline{\gamma}_j}\right)^m \gamma^{m-1} e^{-\left(\frac{m\gamma}{\overline{\gamma}_j}\right)}}{\Gamma(m)} \\ &\quad \times Q_m\left(\sqrt{\frac{2m\rho_{i,j}\gamma}{(1-\rho_{i,j})\overline{\gamma}_j}}, \sqrt{\frac{2m\gamma_T}{(1-\rho_{i,j})\overline{\gamma}_i}}\right) \\ &= p_{\gamma_j}(\gamma) Q_m\left(\sqrt{\frac{2m\rho_{i,j}\gamma}{(1-\rho_{i,j})\overline{\gamma}_j}}, \right. \\ &\qquad \left. \sqrt{\frac{2m\gamma_T}{(1-\rho_{i,j})\overline{\gamma}_i}}\right)\end{aligned} \tag{14}$$

and substituting (14) into (11), $p_{\gamma_{\mathrm{ssc}_\tau}}(\gamma)$ can be rewritten as

$$\begin{aligned}p_{\gamma_{\mathrm{ssc}_\tau}}(\gamma) = p_1(\gamma_T)\left[p_{\gamma_{2\tau}}(\gamma) + \omega_{1,1\tau}(\gamma) - \omega_{1,2\tau}(\gamma)\right] \\ + p_2(\gamma_T)\left[p_{\gamma_{1\tau}}(\gamma) + \omega_{2,2\tau}(\gamma) - \omega_{2,1\tau}(\gamma)\right].\end{aligned} \tag{15}$$

The MGF of $\gamma_{\mathrm{ssc}_\tau}$, defined by

$$\mathcal{M}_{\gamma_{\mathrm{ssc}_\tau}}(s) \triangleq \int_{-\infty}^{\infty} e^{sx} p_{\gamma_{\mathrm{ssc}_\tau}}(x)dx \tag{16}$$

can be expressed as

$$\begin{aligned}\mathcal{M}_{\gamma_{\mathrm{ssc}_\tau}}(s) = & p_1(\gamma_T)\left[\mathcal{M}_{\gamma_{2\tau}}(s) + \Omega_{1,1\tau}(s) - \Omega_{1,2\tau}(s)\right] \\ & + p_2(\gamma_T)\left[\mathcal{M}_{\gamma_{1\tau}}(s) + \Omega_{2,2\tau}(s)\right. \\ & \left. - \Omega_{2,1\tau}(s)\right]\end{aligned} \tag{17}$$

where

$$\Omega_{i,j}(s) \triangleq \int_0^{\infty} e^{s\gamma}\omega_{i,j}(\gamma)d\gamma. \tag{18}$$

Substituting (14) into (18) and using [16, (11)], $\Omega_{i,j}(s)$ can be expressed as

$$\begin{aligned}\Omega_{i,j}(s) = & \left(1 - \frac{\overline{\gamma}_j}{m}s\right)^{-m} \\ & \times \exp\left(-\frac{m\gamma_T}{\overline{\gamma}_i}\frac{1-\frac{s\overline{\gamma}_j}{m}}{1-\frac{s(1-\rho_{i,j})\overline{\gamma}_j}{m}}\right) \\ & \times \sum_{k=0}^{m-1}\frac{1}{k!}\left(\frac{m\gamma_T}{\overline{\gamma}_i}\frac{1-\frac{s\overline{\gamma}_j}{m}}{1-\frac{s(1-\rho_{i,j})\overline{\gamma}_j}{m}}\right).\end{aligned} \tag{19}$$

Now, using [17, (8.352.2)] in (19), we have

$$\Omega_{i,j}(s) = \frac{1}{\Gamma(m)}\left(1-\frac{\overline{\gamma}_j}{m}s\right)^{-m}\Gamma\left(m, \frac{m\gamma_T}{\overline{\gamma}_i}\frac{1-\frac{s\overline{\gamma}_j}{m}}{1-v\frac{s(1-\rho_{i,j})\overline{\gamma}_j}{m}}\right) \tag{20}$$

and, thus

$$\begin{aligned}\mathcal{M}_{\gamma_{\mathrm{ssc}_\tau}}(s) = & p_1(\gamma_T)\left(1-\frac{\overline{\gamma}_{2\tau}}{m}s\right)^{-m} \\ & + p_2(\gamma_T)\left(1-\frac{\overline{\gamma}_{1\tau}}{m}s\right)^{-m} \\ & + \frac{p_1(\gamma_T)}{\Gamma(m)}\left(1-\frac{\overline{\gamma}_{1\tau}}{m}s\right)^{-m} \\ & \times \Gamma\left(m, \frac{m\gamma_T}{\overline{\gamma}_1}\frac{1-\frac{s\overline{\gamma}_{1\tau}}{m}}{1-\frac{s(1-\rho_{1,1\tau})\overline{\gamma}_{1\tau}}{m}}\right) \\ & + \frac{p_2(\gamma_T)}{\Gamma(m)}\left(1-\frac{\overline{\gamma}_{2\tau}}{m}s\right)^{-m} \\ & \times \Gamma\left(m, \frac{m\gamma_T}{\overline{\gamma}_2}\frac{1-\frac{s\overline{\gamma}_{2\tau}}{m}}{1-\frac{s(1-\rho_{2,2\tau})\overline{\gamma}_{2\tau}}{m}}\right) \\ & - \frac{p_1(\gamma_T)}{\Gamma(m)}\left(1-\frac{\overline{\gamma}_{2\tau}}{m}s\right)^{-m} \\ & \times \Gamma\left(m, \frac{m\gamma_T}{\overline{\gamma}_1}\frac{1-\frac{s\overline{\gamma}_{2\tau}}{m}}{1-\frac{s(1-\rho_{1,2\tau})\overline{\gamma}_{2\tau}}{m}}\right) \\ & - \frac{p_2(\gamma_T)}{\Gamma(m)}\left(1-\frac{\overline{\gamma}_{1\tau}}{m}s\right)^{-m} \\ & \times \Gamma\left(m, \frac{m\gamma_T}{\overline{\gamma}_2}\frac{1-\frac{s\overline{\gamma}_{1\tau}}{m}}{1-\frac{s(1-\rho_{2,1\tau})\overline{\gamma}_{1\tau}}{m}}\right).\end{aligned} \tag{21}$$

## III. Analysis of System Performance

In order to have an accurate channel estimation at the receiver, a pilot signal can be sent along with the data bearing signal. The pilot signal can be a tone or multiple tones (PTA) [7], or it can be a sequence of symbols inserted periodically into the data bearing signal (PSA) [8]. The baseband equivalent of the transmitted signal can be expressed as the addition of the baseband data signal and pilot signal, that is

$$x(t) = x_d(t) + x_p(t) \tag{22}$$

with

$$x_d(t) = \begin{cases}\sum_{i=-\infty}^{\infty} x_i q(t-iT_s), & \text{PTA} \\ \sum_{l=-\infty}^{\infty}\sum_{i=1}^{K-1} x_{l(K-1)+i-1} & \\ \quad \times q\left(t-(lK+i)T_m\right), & \text{PSA}\end{cases} \tag{23}$$

$$x_p(t) = \begin{cases}B, & \text{PTA} \\ \sum_{l=-\infty}^{\infty} Be^{\theta}q(t-lKT_m), & \text{PSA}\end{cases} \tag{24}$$

where $x_i = Ae^{j\phi_i}$ denotes the $i$th $M$-ary phase-shift keying (MPSK) transmitted symbol, $T_s$ and $T_m = T_s(K-1)/K$ represent the signalling periods for PTA and PSA systems, respectively, $B$ is the amplitude of the pilot tone signal, $Be^{\theta}$ represents the redundant pilot reference symbol inserted every $(K-1)$ MPSK information symbols within the transmitted data signal sequence, and $q(t)$ is the complex impulse response of a pulse shaping filter. We normalize the energy of the pulse $q(t)$ such that $\int_{-\infty}^{\infty}|q(t)|^2dt = 1$.

Assuming a dual-branch diversity system, the baseband equivalent of the received signal can be expressed as

$$r(t) = \chi_{\mathrm{ssc}_\tau}(t)x(t) + \mu(t) \tag{25}$$

where $\mu(t)$, which represents the additive thermal noise at the receiver front end, is a zero-mean complex Gaussian noise process with single-sided power spectral density $N_0$ and

$$\chi_{\mathrm{ssc}_\tau}(t) = \begin{cases} \chi_{1\tau}(t), & \text{if Rx connected to antenna 1} \\ \chi_{2\tau}(t), & \text{if Rx connected to antenna 2} \end{cases} \tag{26}$$

with $\chi_{k\tau}(t)$ denoting the multiplicative Nakagami-$m$ fading characteristic of the $k$th diversity channel. Under the assumption of nonindependence between diversity branches, the correlation function between the complex channel weights of the antennas can be modeled with the following Bessel model [4]:

$$E\left\{\chi_{1\tau}(t)\chi^*_{2\tau}(t)\right\} = J_0(2\pi d_a) \tag{27}$$

where $J_0(\cdot)$ is the Bessel function of order zero and $d_a$ is the normalized distance between antennas.

As shown in Fig. 1, the received data signal is passed to a matched filter with an impulse response equal to $q^*(-t)$ and the phase reference is extracted by suitable filtering/interpolation means. The received data signal and phase reference after matched filtering/interpolation can be written as

$$w(t) = \chi_{\mathrm{ssc}_\tau}(t)x_d(t) * q^*(-t) + n(t) \tag{28}$$

$$p(t) = \chi_{\mathrm{ssc}}(t)x_p(t) * h_p(t) + \upsilon(t) \tag{29}$$

respectively, where $n(t)$ and $\upsilon(t)$ are uncorrelated zero mean complex Gaussian noise processes and $h_p(t)$ represents the impulse response of the pilot extraction/interpolation filter.

Assuming a perfect clock recovery and that $h(t) = q(t) * q^*(-t)$ satisfies Nyquist's criterion for zero intersymbol interference, the complex samples at the MPSK detector input at time $t = iT_s$ will be given by

$$w_i = \chi_{\mathrm{ssc}_\tau, i}x_i + n_i \tag{30}$$

$$p_i = \chi_{\mathrm{ssc}, i}B + \upsilon_i. \tag{31}$$

A maximum a-posteriori probability receiver employing coherent detection of equiprobable, equal energy MPSK signals will determine the phase angle $\psi$ between the two vectors $w_i$ and $p_i$ and decide in favor of the symbol $\hat{x}_i$ whose phase is closest to $\psi$. By conditioning on the fading, the random variables $w_i$ and $p_i$ are two vectors perturbed by uncorrelated Gaussian noise. In this case, as shown by Pawula *et al.* in [18] and [19], the conditional symbol error probability can be written as

$$\begin{aligned} P_s\left(\gamma_{\mathrm{ssc}_\tau}\right) &= \frac{1}{\pi}\int_0^{\frac{(M-1)\pi}{M}} \exp\left[-\frac{\rho_w\rho_p\sin^2(\frac{\pi}{M})}{\rho_w\sin^2\varphi + \rho_p\sin^2\left(\varphi+\frac{\pi}{M}\right)}\right]d\varphi \\ &= \frac{1}{\pi}\int_0^{\frac{(M-1)\pi}{M}} \exp[\Upsilon(\varphi)\gamma_{\mathrm{ssc}_\tau}]d\varphi \end{aligned} \tag{32}$$

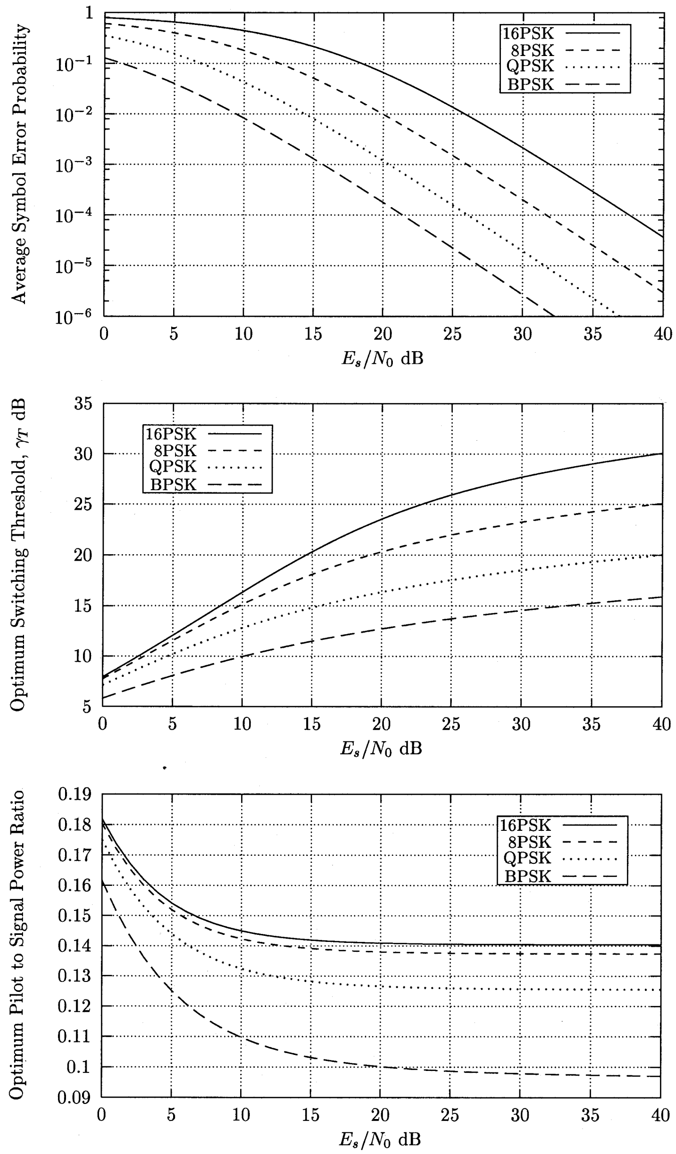


Fig. 2. Optimum performance, optimum switching threshold and optimum pilot-to-signal power ratio versus $E_s/N_0$ on each branch for a Nakagami-$m$ fading with $m = 1$ and $f_dT_s = 0.01$, a normalized distance between antennas $d_a = 0.3$, and for different values of alphabet cardinality $M$.

with

$$\Upsilon(\varphi) = -\frac{\alpha_w\alpha_p\sin^2(\frac{\pi}{M})}{\frac{\alpha_w}{rP_w}\sin^2\varphi + \frac{r\alpha_p}{P_p}\sin^2\left(\varphi+\frac{\pi}{M}\right)}$$

where it has been assumed that

$$\rho_w = \frac{A^2\left|\chi_{\mathrm{ssc}_\tau, i}\right|^2}{2N_0} = P_w\alpha_w\gamma_{\mathrm{ssc}_\tau} \tag{33}$$

$$\rho_p = \frac{B^2|\chi_{\mathrm{ssc}, i}|^2}{2N_p} = P_p\alpha_p\gamma_{\mathrm{ssc}_\tau} \tag{34}$$

where $N_p$ denotes the variance of $\upsilon_i$ that depends on the type of filter/interpolator used for the pilot reference recovery, $P_w$ represents the transmitted signal power, $P_p$ denotes the transmitted pilot power, $r \triangleq P_p/P_w$ is defined as the pilot-to-signal power ratio, and $\alpha_w$ and $\alpha_p$ represent variables that depend on the type of reference-based system.

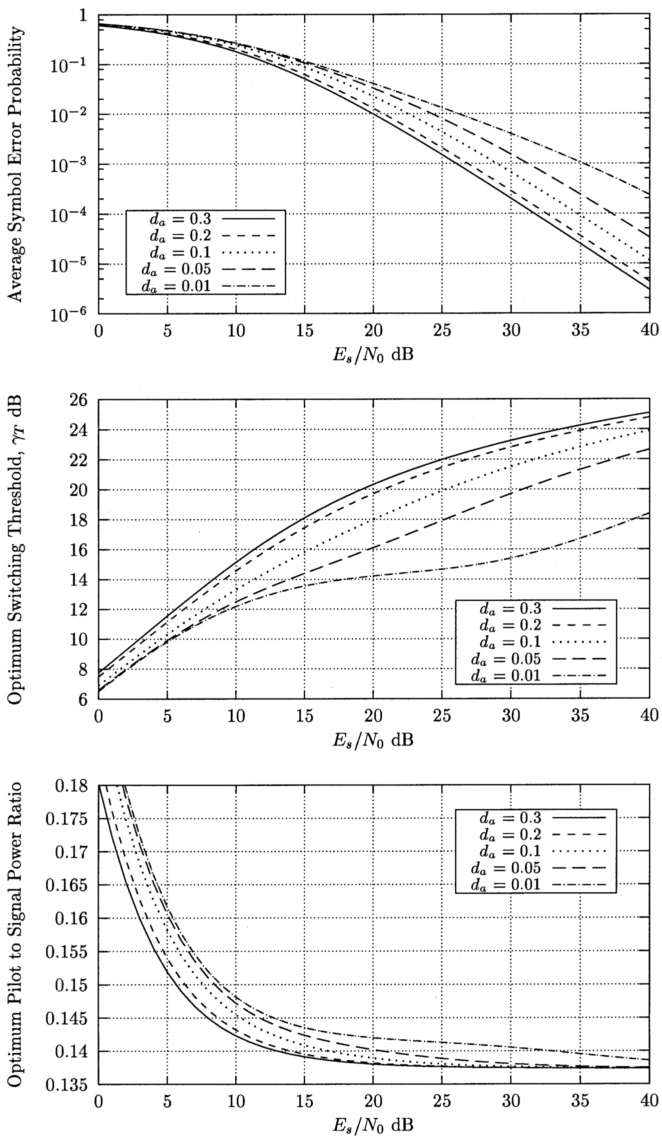


Fig. 3. Optimum performance, optimum switching threshold, and optimum pilot-to-signal power ratio versus $E_s/N_0$ on each branch for an 8PSK modulation scheme, a Nakagami-$m$ fading with $m = 1$ and $f_dT_s = 0.01$, and for different values of the normalized distance between antennas $d_a$.

The average symbol error rate (SER) $P_s$ for the problem at hand can be written as

$$P_s = \int_{-\infty}^{\infty} P_s(\gamma) p_{\gamma_{\mathrm{ssc}_\tau}}(\gamma) d\gamma. \tag{35}$$

By substituting (32) in (35) and then interchanging the order of integration, and recognizing that the integral with respect to $\gamma$ is equal to the MGF of $\gamma_{\mathrm{ssc}_\tau}$ evaluated at $s = \Upsilon(\varphi)$, (35) reduces to

$$P_s = \frac{1}{\pi} \int_{0}^{\frac{(M-1)\pi}{M}} \mathcal{M}_{\gamma_{\mathrm{ssc}_\tau}} \left[\Upsilon(\varphi)\right] d\varphi. \tag{36}$$

This expression can be easily evaluated to any degree of accuracy by several numerical integration methods. In particular, the change of variables $x = \cos(M\varphi/(M-1))$ enables us to use the Gauss–Chebyshev quadrature rules [20, 25.4.38], which have the advantage that their abscissas and weights admit a closed-form expression. In this way, after some algebraic manipulations, we obtain

$$\begin{aligned} P_s &= \frac{M-1}{\pi M} \int_{-1}^{1} \mathcal{M}_{\gamma_{\mathrm{ssc}_\tau}} \left[\Upsilon\left(\frac{M-1}{M} \arccos x\right)\right] \frac{dx}{\sqrt{1-x^2}} \\ &= \frac{M-1}{nM} \sum_{l=1}^{n} \\ &\quad \mathcal{M}_{\gamma_{\mathrm{ssc}_\tau}} \left[\Upsilon\left(\frac{(M-1)(2l-1)\pi}{2nM}\right)\right] + R_n \end{aligned} \tag{37}$$

where $n$ is a small positive integer, and the remainder term can be expressed as [20, 25.4.38]

$$R_n = \frac{(M-1)}{M(2n)!2^{2n-1}} \mathcal{M}^{(2n)}_{\gamma_{\mathrm{ssc}_\tau}}(\xi) \tag{38}$$

for some $-1 < \xi < 1$. Notation $\mathcal{M}^{(2n)}_{\gamma_{\mathrm{ssc}_\tau}}(s)$ is used to denote the $2n$th derivative of $\mathcal{M}_{\gamma_{\mathrm{ssc}_\tau}}(s)$.

### A. Optimum Adaptive Strategy (OAS)

As is shown in (35)–(37), the average SER depends not only on the modulation alphabet cardinality, the channel fading severity, the correlation coefficient between diversity antennas, and the correlation coefficient between matched filter and pilot extraction filter outputs but also on the values of the switching threshold $\gamma_T$ and the pilot-to-signal power ratio $r$. As the average SER is a continuous function of $\gamma_T$ and $r$, there exist optimal values of $\gamma_T$ and $r$ for which the average SER is minimal. These optimal values $\gamma_T^{\mathrm{OAS}}$ and $r^{\mathrm{OAS}}$ are a solution of the system

$$\left.\frac{\partial P_s}{\partial \gamma_T}\right|_{\gamma_T=\gamma_T^{\mathrm{OAS}},\ r=r^{\mathrm{OAS}}} = 0, \qquad \left.\frac{\partial P_s}{\partial r}\right|_{\gamma_T=\gamma_T^{\mathrm{OAS}},\ r=r^{\mathrm{OAS}}} = 0. \tag{39}$$

In general, to find the optimum values of the switching threshold and the pilot-to-signal power ratio, (39) must be solved numerically. Nevertheless, in some particular cases that will be solved latter in this paper, it is possible to obtain closed-form expressions for $\gamma_T^{\mathrm{OAS}}$ and/or $r^{\mathrm{OAS}}$ in terms of $M$, $m$, $E_s/N_0$, $\rho_{1,1\tau}$, $\rho_{2,2\tau}$, $\rho_{1,2\tau}$, and $\rho_{2,1\tau}$.

### B. Optimum Fixed Strategies

As is shown in Section III-A, given the MPSK alphabet cardinality, the optimum adaptive switching threshold and the optimum pilot-to-signal power ratio could only be achieved by adapting $\gamma_T$ and $r$ to the actual values of channel fading severity, average SNR at the matched filter and pilot extraction filter outputs, correlation coefficient between antennas, and correlation coefficient between matched filter output and pilot extraction filter output. However, in most applications, particularly in wireless communication systems, this could be a very difficult task. Then, in practical conditions, it can be appropriate to use fixed switching threshold and pilot-to-signal power ratio, which are independent of the actual values of system parameters. In order to set a fixed threshold and a fixed pilot-to-signal power ratio, it is possible to use different criteria that give rise to different

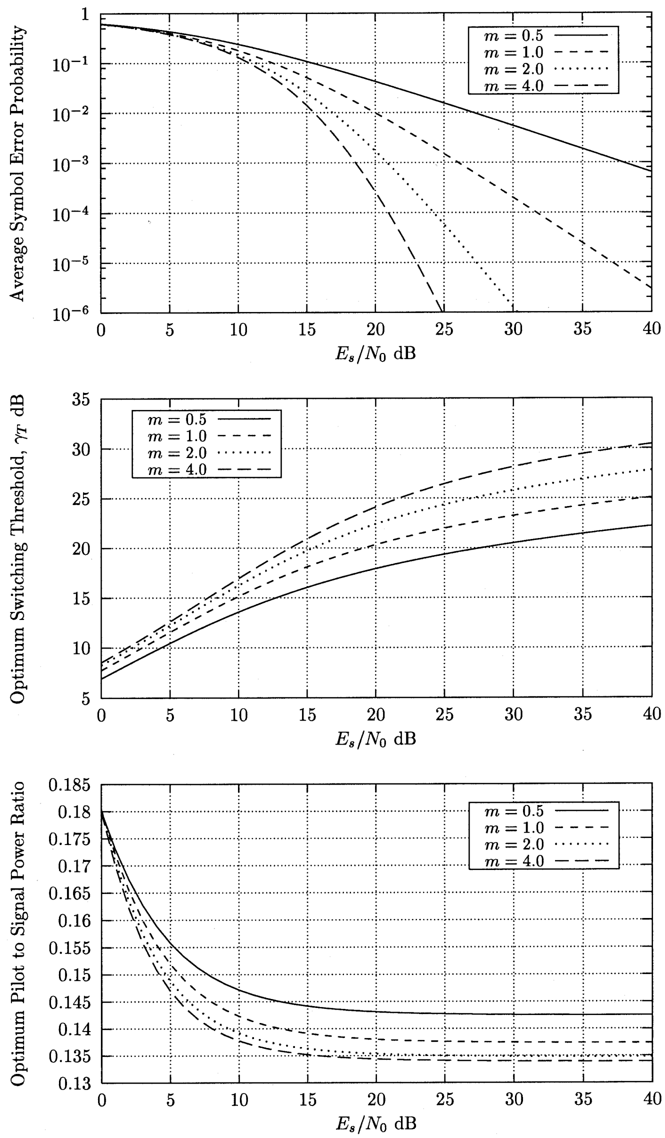


Fig. 4. Optimum performance, optimum switching threshold, and optimum pilot-to-signal power ratio versus $E_s/N_0$ on each branch for an 8PSK modulation scheme, a normalized distance between antennas $d_a = 0.3$, and a Nakagami-$m$ fading with $f_dT_s = 0.01$ and different values of $m$.

strategies. Based on the framework developed by Fedele in [12] three different strategies are presented.

a) *Minimum Cost Strategy (MCS):* The fixed switching threshold and the fixed pilot-to-signal power ratio are evaluated as the values $\gamma_T^{\mathrm{MCS}}$ and $r^{\mathrm{MCS}}$ that, given an alphabet cardinality $M$ and a normalized distance between antennas $d_a$, minimize, for example, the cost function defined as the logarithm of the root mean square error between the average SERs $P_s(\gamma_T, r, E_s/N_0, m, f_dT_s)$ and $P_s(\gamma_T^{\mathrm{OAS}}, r^{\mathrm{OAS}}, E_s/N_0, m, f_dT_s)$. That is

$$C(\gamma_T, r) \triangleq \int_{\left(\frac{E_s}{N_0}\right)_1}^{\left(\frac{E_s}{N_0}\right)_2} \int_{m_1}^{m_2} \int_{f_{d,1}T_s}^{f_{d,2}T_s} \times \log\left[\frac{P_s(\gamma_T, r, \beta, \vartheta, \zeta)}{P_s\left(\gamma_T^{\mathrm{OAS}}, r^{\mathrm{OAS}}, \beta, \vartheta, \zeta\right)}\right] d\zeta d\vartheta d\beta. \tag{40}$$

b) *Fixed Average Strategy (FAS):* The fixed threshold $\gamma_T^{\mathrm{FAS}}$ and the fixed pilot-to-signal power ratio $r^{\mathrm{FAS}}$ are obtained as the average values of $\gamma_T^{\mathrm{OAS}}$ and $r^{\mathrm{OAS}}$ over the $E_s/N_0$ interval $[(E_s/N_0)_1, (E_s/N_0)_2]$, the $m$ interval $(m_1, m_2)$, and the $f_dT_s$ interval $(f_{d,1}T_s,\, f_{d,2}T_s)$. That is

$$\gamma_T^{\mathrm{FAS}} \triangleq \frac{1}{\Delta} \int_{\left(\frac{E_s}{N_0}\right)_1}^{\left(\frac{E_s}{N_0}\right)_2} \int_{m_1}^{m_2} \int_{f_{d,1}T_s}^{f_{d,2}T_s} \gamma_T^{\mathrm{OAS}}(\beta, \vartheta, \zeta) d\zeta d\vartheta d\beta$$

$$r^{\mathrm{FAS}} \triangleq \frac{1}{\Delta} \int_{\left(\frac{E_s}{N_0}\right)_1}^{\left(\frac{E_s}{N_0}\right)_2} \int_{m_1}^{m_2} \int_{f_{d,1}T_s}^{f_{d,2}T_s} r^{\mathrm{OAS}}(\beta, \vartheta, \zeta) d\zeta d\vartheta d\beta \tag{41}$$

where we have assumed uniform distributions of these parameters over the corresponding optimization intervals, and thus, $\Delta = [(E_s/N_0)_2 - (E_s/N_0)_1] \cdot (m_2 - m_1) \cdot (f_{d,2}T_s - f_{d,1}T_s)$.

c) *Midpoint Strategy (MPS):* The system is operated with the fixed parameters

$$\begin{aligned} \gamma_T^{\mathrm{MPS}} &= \gamma_T^{\mathrm{OAS}}(\beta_{mp}, \vartheta_{mp}, \zeta_{mp}) \\ r^{\mathrm{MPS}} &= r^{\mathrm{OAS}}(\beta_{mp}, \vartheta_{mp}, \zeta_{mp}) \end{aligned} \tag{42}$$

where $\beta_{mp} = [(E_s/N_0)_1 + (E_s/N_0)_2]/2$, $\vartheta_{mp} = (m_1 + m_2)/2$, and $\zeta_{mp} = (f_{d,1}T_s + f_{d,2}T_s)/2$.

## IV. Pilot-Tone-Aided MPSK System

In this case, the channel estimator is simply a pilot extraction filter with a frequency response

$$H_p(f) = \begin{cases} 1, & -\frac{B_p}{2} \le f \le \frac{B_p}{2} \\ 0, & \text{otherwise.} \end{cases} \tag{43}$$

It is assumed that the power spectrum of the data bearing signal has a spectral null that allows for the insertion and the extraction of the pilot. The bandwidth of the filter must be wide enough to allow the fading to pass through undistorted, that is, it must be at least twice the maximum Doppler shift $f_d$. In the following analysis, it will be assumed that a filter with bandwidth $B_p = 2f_d$ is used. Thus, the data bearing signal and the pilot signal at the output of the matched filter and pilot extraction filter can be expressed as

$$w(t) = \chi_{\mathrm{ssc}_\tau}(t) \sum_i x_i h(t - iT_s) + n(t) \tag{44}$$

$$p(t) = \chi_{\mathrm{ssc}_\tau}(t) B + \upsilon(t) \tag{45}$$

respectively, where $h(t) = q(t) * q^*(-t)$ represents the overall impulse response of the system for a perfect nonselective transmission medium and $n(t)$ and $\upsilon(t)$ are zero-mean complex Gaussian noise processes. Note that $n(t)$ is independent of $\upsilon(t)$ due to the fact that they are output noise processes of two filters whose frequency responses do not overlap. Assuming a perfect clock recovery, the complex samples at the MPSK detector input at time $t = iT_s$ will be given by

$$w_i = \chi_{\mathrm{ssc}_\tau, i} x_i + n_i \tag{46}$$

$$p_i = \chi_{\mathrm{ssc}_\tau, i} B + \upsilon_i \tag{47}$$

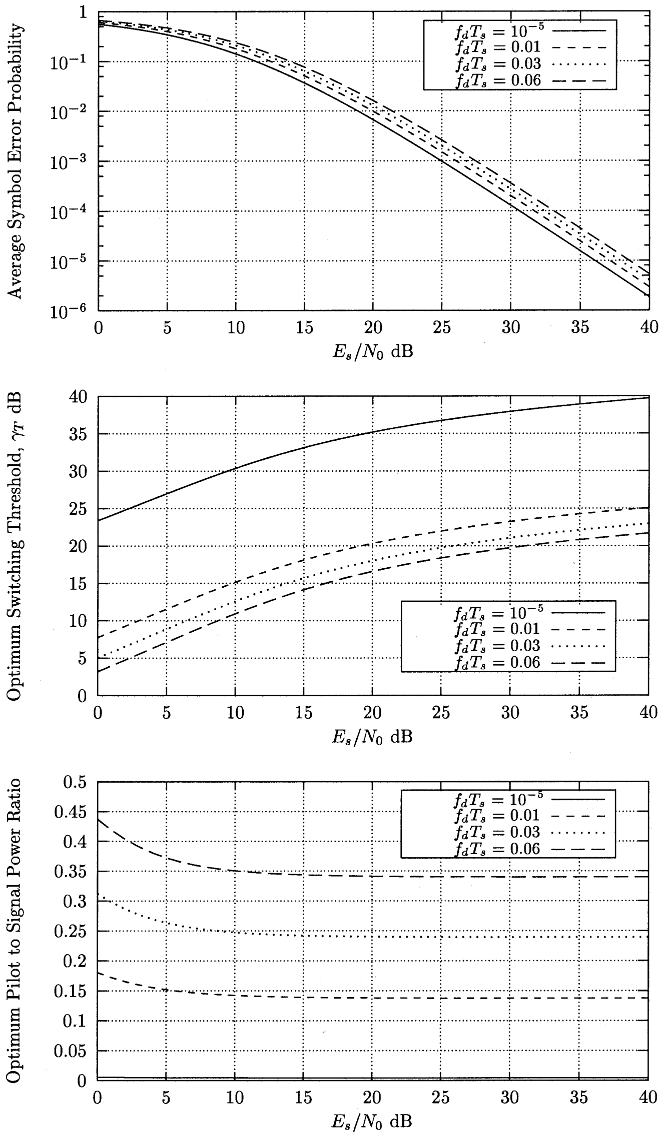


Fig. 5. Optimum performance, optimum switching threshold, and optimum pilot-to-signal power ratio versus $E_s/N_0$ on each branch for an 8PSK modulation scheme, a normalized distance between antennas $d_a = 0.3$, and a Nakagami-$m$ fading with $m = 1$ and different values of $f_dT_s$.

and, thus

$$\rho_w = \frac{A^2\left|\chi_{\mathrm{ssc}_\tau,i}\right|^2}{2N_0} = \gamma_{\mathrm{ssc}_\tau} \Rightarrow \alpha_w = \frac{1}{P_w} \tag{48}$$

$$\rho_p = \frac{B^2\left|\chi_{\mathrm{ssc}_\tau,i}\right|^2}{2N_0B_p} = \frac{B^2}{A^2B_p}\gamma_{\mathrm{ssc}_\tau} \Rightarrow \alpha_p = \frac{B^2}{A^2B_pP_p}. \tag{49}$$

Using (37), the average SER can then be written as

$$P_s \simeq \frac{M-1}{nM} \times \sum_{l=1}^{n} \mathcal{M}_{\gamma_{\mathrm{ssc}_\tau}}\left[\frac{-\sin^2\left(\frac{\pi}{M}\right)}{\frac{A^2B_p}{B^2}\sin^2(\kappa_l) + \sin^2\left(\kappa_l + \frac{\pi}{M}\right)}\right] \tag{50}$$

where $\kappa_l = (M-1)(2l-1)\pi/2nM$.

Under Nakagami-$m$ slow fading conditions, $\gamma_k$ and $\gamma_{k\tau}$ ($k = 1, 2$) can be expressed as

$$\gamma_k = \frac{B^2|\chi_k|^2}{2N_0B_p} \tag{51}$$

$$\gamma_{k\tau} = \frac{A^2|\chi_k|^2}{2N_0} \tag{52}$$

$$\overline{\gamma}_k = \frac{B^2}{2N_0B_p} = \frac{r\frac{E_s}{N_0}}{(1+r)B_pT_s}$$
$$\overline{\gamma}_{k\tau} = \frac{A^2}{2N_0} = \frac{\frac{E_s}{N_0}}{1+r} \tag{53}$$

$$\rho_{1,2\tau} = \rho_{2,1\tau} \triangleq \frac{E\{\gamma_1\gamma_{2\tau}\}}{2\sqrt{E\left\{\gamma_1^2\right\}E\left\{\gamma_{2\tau}^2\right\}}} = J_0^2(2\pi d_a) \tag{54}$$

$$\rho_{k,k\tau} \triangleq \frac{E\{\gamma_k\gamma_{k\tau}\}}{2\sqrt{E\left\{\gamma_k^2\right\}E\left\{\gamma_{k\tau}^2\right\}}} = 1 \tag{55}$$

with $E_s = (A^2 + B^2T_s)/2$ and $r = B^2T_s/A^2$ being the equivalent energy per MPSK symbol and the pilot-to-signal power ratio, respectively. Using (53)–(55) in (21) and (50), the expression of $P_s$ reduces after some simplifications to

$$P_s \simeq \frac{M-1}{nM}\sum_{l=1}^{n}\left(1+\frac{\alpha_l\frac{E_s}{N_0}}{m(1+r)}\right)^{-m} \times \left[1+\frac{\Gamma\left(m, \frac{\gamma_T B_p T_s\left[m(1+r)+\alpha_l\frac{E_s}{N_0}\right]}{r\frac{E_s}{N_0}}\right)}{\Gamma(m)} - \frac{\Gamma\left(m, \frac{m\gamma_T B_p T_s(1+r)\left[m(1+r)+\alpha_l\frac{E_s}{N_0}\right]}{r\left[m(1+r)+\alpha_l\left[1-J_0^2(2\pi d_a)\right]\frac{E_s}{N_0}\right]\frac{E_s}{N_0}}\right)}{\Gamma(m)}\right] \tag{56}$$

where

$$\alpha_l \triangleq \frac{\sin^2\left(\frac{\pi}{M}\right)}{\frac{r}{B_pT_s}\sin^2(\kappa_l)+\sin^2\left(\kappa_l+\frac{\pi}{M}\right)}. \tag{57}$$

### *A. Optimum Adaptive Performance*

Figs. 2–5 show the minimum average SER, the optimum switching threshold, and the optimum pilot-to-signal power ratio versus the $E_s/N_0$ on each branch. As shown in Fig. 2, when the cardinality of the MPSK symbol alphabet increases, the decision regions for phase detection, defined by $[(2i-1)\pi/M, (2i+1)\pi/M]$, $i = 0, 1, 2, \ldots, (M-1)$, become smaller, thus increasing the average SER. Furthermore, for a fixed value of Nakagami-$m$ fading parameter $m$, normalized maximum Doppler shift $f_dT_s$, and normalized distance between antennas $d_a$, both the optimum switching threshold and the optimum pilot-to-signal power ratio are an increasing function of the MPSK alphabet cardinality $M$. For fixed $M$, $m$, and $f_dT_s$, the optimum switching threshold increases with $E_s/N_0$ and the optimum pilot-to-signal power ratio decreases with $E_s/N_0$.

Similarly, as shown in Fig. 3, given a modulation scheme (in this case 8PSK) and for fixed value of Nakagami-$m$ fading

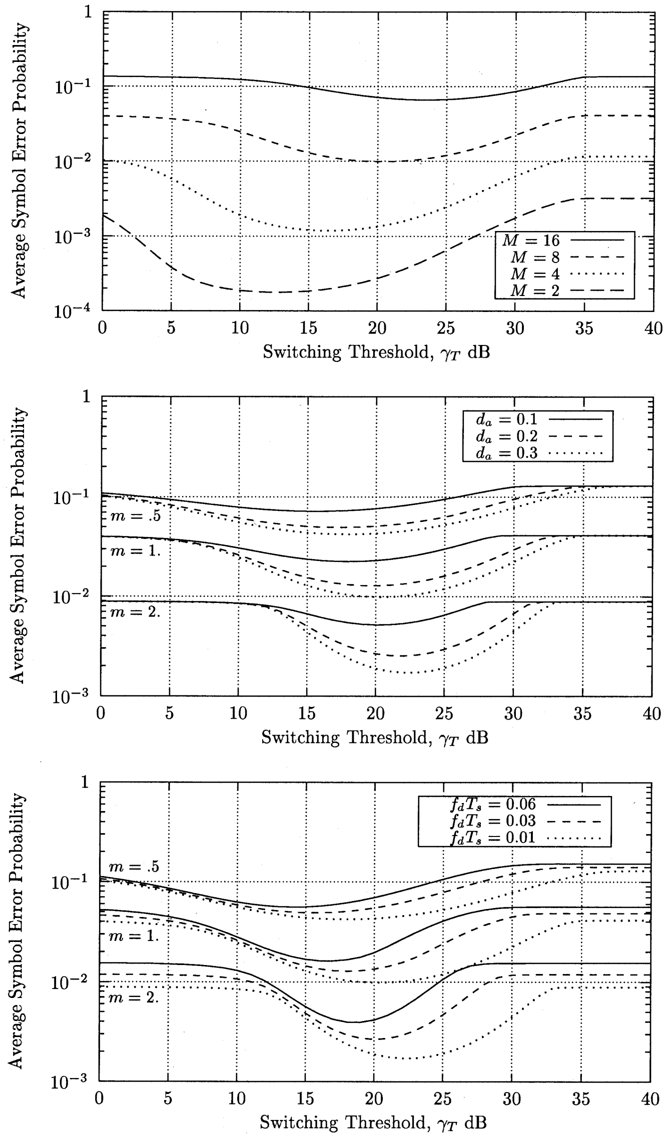


Fig. 6. Optimum (with respect to $r$) average symbol error rate versus switching threshold at a fixed $E_s/N_0 = 20\ dB$ on each branch for different values of alphabet cardinality $M$, normalized distance between antennas $d_a$, and Nakagami fading parameters $m$ and $f_dT_s$. Where not specified, $M = 8$, $d_a = 0.3$, $m = 1$, and $f_dT_s = 0.01$.

parameter $m$ and normalized maximum Doppler shift $f_dT_s$, the optimum switching threshold is an increasing function of the normalized distance between antennas $d_a$ and the optimum pilot-to-signal power ratio is a decreasing function of $d_a$. As $d_a$ tends to zero (totally correlated antennas), the optimum average SER tends to equal that of a single branch receiver. Thus, the results show that, in the range of SER values of practical interest, a diversity gain of several dBs can be obtained for normalized distances between antennas greater than $d_a = 0.05$.

The effect of Nakagami-$m$ fading conditions on the minimum average SER, the optimum switching threshold, and the optimum pilot-to-signal power ratio is analyzed in Figs. 4 and 5. In particular, as expected, the performance improves as $m$ increases, since the fading becomes less severe, and deteriorates as $f_dT_s$ increases, since the bandwidth of the pilot tone extraction filter must be wide enough to allow the fading to pass through undistorted and, thus, the reference signal at the output of the filter is noisier. Furthermore, as shown in Fig. 4, given a modulation scheme (in this case 8PSK) and for fixed value of normalized distance between antennas $d_a$ and normalized maximum Doppler shift $f_dT_s$, the optimum switching threshold is an increasing function of the fading parameter $m$ and the optimum pilot-to-signal power ratio is a decreasing function of $m$. Also, as shown in Fig. 5, given a modulation scheme (in this case 8PSK) and for fixed value of normalized distance between antennas $d_a$ and Nakagami-$m$ fading parameter $m$, the optimum switching threshold is a decreasing function of the normalized Doppler shift $f_dT_s$ and the optimum pilot-to-signal power ratio is an increasing function of $f_dT_s$.

It is also interesting to consider the sensitivity of the average SER to the value of the switching threshold and the value of the pilot-to-signal power ratio. To this end, for a fixed average $E_s/N_0 = 20\ dB$ on each branch, Figs. 6 and 7 show the optimum (with respect to $r$) average SER versus switching threshold and the optimum (with respect to $\gamma_T$) average SER versus pilot-to-signal power ratio, respectively, for different values of alphabet cardinality $M$, normalized distance between antennas $d_a$, and Nakagami fading parameters $m$ and $f_dT_s$. The more the fading parameter increases, the less sensitive is the average SER to switching threshold and pilot-to-signal power ratio variations around the optimum values, independently of the normalized distance between antennas and/or the normalized Doppler frequency of the fading. Moreover, in less severe fading conditions, the sensitivity to $\gamma_T$ and $r$ increases, especially in slow fading conditions.

### B. Optimum Nonadaptive Performance

Table I shows the values of the fixed thresholds and fixed pilot-to-signal power ratios obtained by the application of the proposed strategies (MCS, FAS, and MPS) for different values of alphabet cardinality $M$ and normalized distance between antennas $d_a$. In order to determine the values of $\gamma_T^{\mathrm{MCS}}$ and $r^{\mathrm{MCS}}$, the cost function $C(\gamma_T, r)$ has been numerically minimized. In fact, the triple integral in (40) has been computed numerically over the intervals $[m_1, m_2] = [0.5, 2.0]$, $[f_{d,1}T_s, f_{d,2}T_s] = [0.01, 0.06]$, with $[(E_s/N_0)_1, (E_s/N_0)_2]$ being equal to [10 dB, 30 dB] for binary phase-shift keying (BPSK), [15 dB, 35 dB] for quaternary phase-shift keying (QPSK), [20 dB, 40 dB] for 8PSK, and [25 dB, 45 dB] for 16PSK. The values of $\gamma_T^{\mathrm{FAS}}$ and $r^{\mathrm{FAS}}$ have also been obtained through numerical computation of the triple integrals in (41) over the same intervals. Finally, the values of $\gamma_T^{\mathrm{MPS}}$ and $r^{\mathrm{MPS}}$ have been obtained using (42) with $\vartheta_{mp} = 1.25$, $\zeta_{mp} = 0.035$, and $\beta_{mp}$ being equal to 20 dB for BPSK, 25 dB for QPSK, 30 dB for 8PSK, and 40 dB for 16PSK. The results show that for a fixed value of the normalized distance between antennas $d_a$, the fixed switching threshold and the fixed pilot-to-signal power ratio are increasing functions of the MPSK alphabet cardinality $M$, independent of the adopted optimum fixed strategy. Furthermore, for a fixed value of $M$, the fixed switching threshold increases with $d_a$ and the optimum pilot-to-signal power ratio is almost constant.

With reference to the fixed switching thresholds $\gamma_T^{\mathrm{MCS}}$, $\gamma_T^{\mathrm{FAS}}$, and $\gamma_T^{\mathrm{MPS}}$ and the fixed pilot-to-signal power ratios $r^{\mathrm{MCS}}$, $r^{\mathrm{FAS}}$, and $r^{\mathrm{MPS}}$ of Table I, Fig. 8 shows the average SER

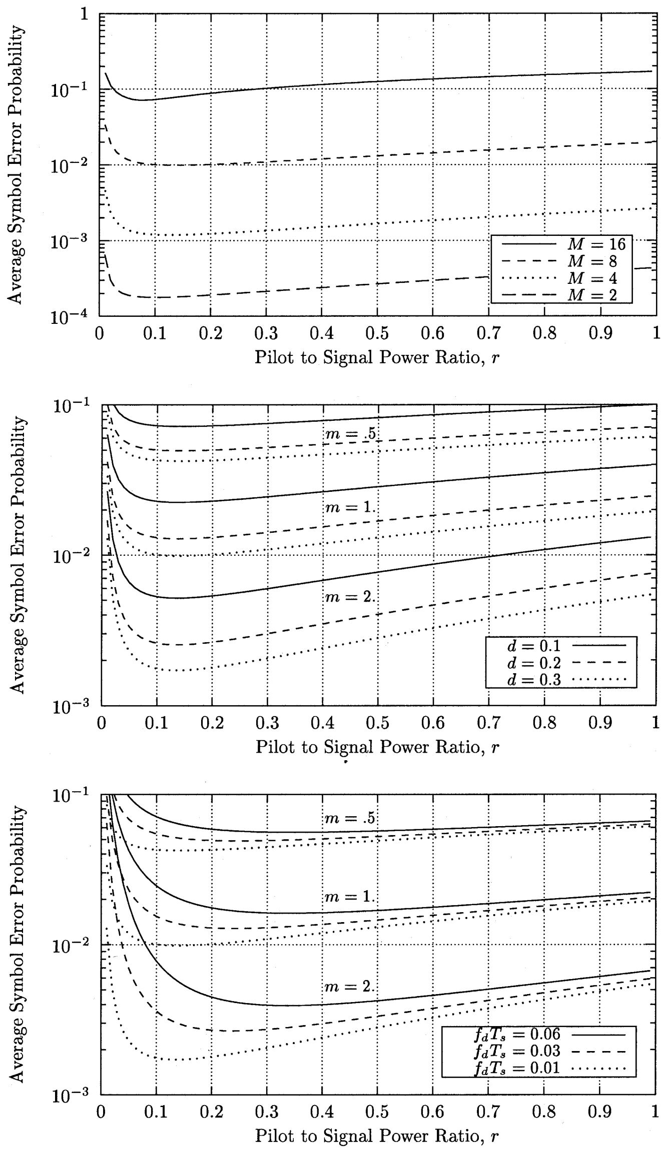


Fig. 7. Optimum (with respect to $\gamma_T$) average symbol error rate versus pilot-to-signal power ratio at a fixed $E_s/N_0 = 20\ dB$ on each branch for different values of alphabet cardinality $M$, normalized distance between antennas $d_a$, and Nakagami fading parameters $m$ and $f_dT_s$. Where not specified, $M = 8$, $d_a = 0.3$, $m = 1$, and $f_dT_s = 0.01$.

versus $E_s/N_0$ on each branch for different values of alphabet cardinality and for $m = 1.$, $f_dT_s = 0.03$, and $d_a = 0.3$. For comparison purposes, the optimum performance (OAS) of the system is also presented. As can be seen, the SER performances of FAS and MPS are very close to each other. They differ with respect to the SER performance of MCS in that the former provides accurate results for high values of SER and the latter provides accurate results for low values of SER. Similarly, given a modulation scheme (in this case 8PSK) and for fixed value of Nakagami-$m$ fading severity $m = 1$ and normalized maximum Doppler shift $f_dT_s = 0.03$, Fig. 9 shows the average SER versus $E_s/N_0$ on each branch for different values of $d_a$.

The effect of Nakagami-$m$ fading conditions on the average SER is analyzed in Fig. 10, where the average SER versus $E_s/N_0$ on each branch for $M = 8$, $d_a = 0.3$, $m = 0.5, 1, 2,$

TABLE I

FIXED SWITCHING THRESHOLDS AND SIGNAL-TO-PILOT POWER RATIOS FOR BPSK, QPSK, 8PSK, AND 16PSK WITH $m_1 = 0.5$, $m_2 = 2.0$, $f_{d,1}T_s = 0.01$, AND $f_{d,2}T_s = 0.06$. THE INTERVAL $[(E_s/N_0)_1, (E_s/N_0)_2]$ IS: [10 dB, 30 dB] FOR BPSK, [15 dB, 35 dB] FOR QPSK, [20 dB, 40 dB] FOR 8PSK, AND [25 dB, 45 dB] FOR 16PSK

| $M$ | $d_a$ | MCS | | FAS | | MPS | |
|---|---|---|---|---|---|---|---|
| | | $\gamma_T^{MCS}$ | $r^{MCS}$ | $\gamma_T^{FAS}$ | $r^{FAS}$ | $\gamma_T^{MPS}$ | $r^{MPS}$ |
| 2 | 0.1 | 9.3 | 0.132 | 8.6 | 0.189 | 8.9 | 0.190 |
| | 0.2 | 10.7 | 0.128 | 9.9 | 0.186 | 10.2 | 0.182 |
| | 0.3 | 11.1 | 0.126 | 10.4 | 0.184 | 10.6 | 0.179 |
| 4 | 0.1 | 13.5 | 0.135 | 13.7 | 0.233 | 14.1 | 0.238 |
| | 0.2 | 14.9 | 0.134 | 15.1 | 0.232 | 15.4 | 0.237 |
| | 0.3 | 15.3 | 0.134 | 15.5 | 0.232 | 15.8 | 0.236 |
| 8 | 0.1 | 19.4 | 0.143 | 19.4 | 0.250 | 19.8 | 0.257 |
| | 0.2 | 20.4 | 0.143 | 20.7 | 0.250 | 21.1 | 0.257 |
| | 0.3 | 20.8 | 0.143 | 21.2 | 0.250 | 21.6 | 0.257 |
| 16 | 0.1 | 24.9 | 0.150 | 25.0 | 0.254 | 25.5 | 0.263 |
| | 0.2 | 26.2 | 0.150 | 26.4 | 0.254 | 26.9 | 0.263 |
| | 0.3 | 26.7 | 0.150 | 26.9 | 0.254 | 27.4 | 0.263 |

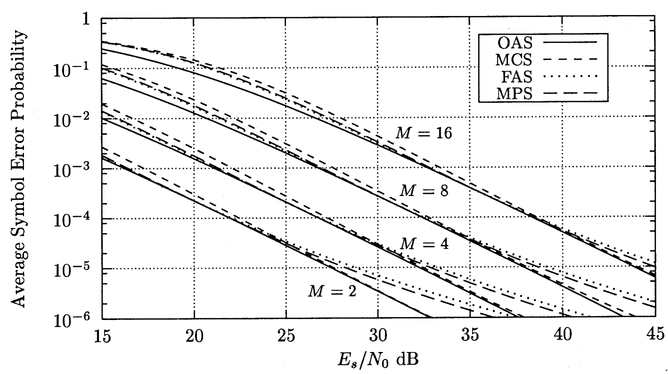


Fig. 8. Average symbol error rate versus $E_s/N_0$ per symbol on each branch for different values of alphabet cardinality $M$ and for $d_a = 0.3$, $m = 1$, and $f_dT_s = 0.03$. Fixed switching thresholds and pilot-to-signal power ratios (Table I) are used. The optimum performance (OAS) of the system is also presented.

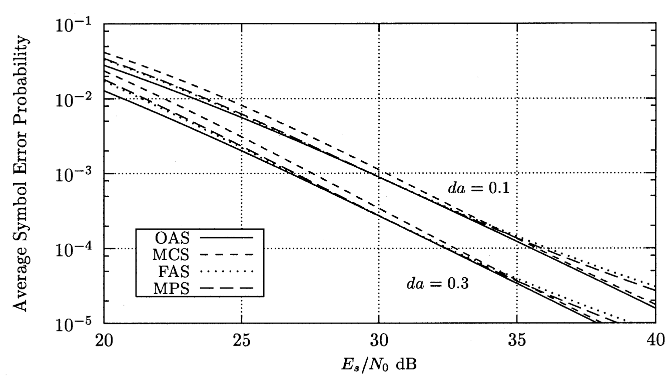


Fig. 9. Average symbol error rate versus $E_s/N_0$ per symbol on each branch for an 8PSK modulation scheme, a Nakagami-$m$ fading channel with $m = 1$ and $f_dT_s = 0.03$, and for different values of normalized distance between antennas $d_a$. Fixed switching thresholds and pilot-to-signal power ratios (Table I) are used. The optimum performance (OAS) of the system is also presented.

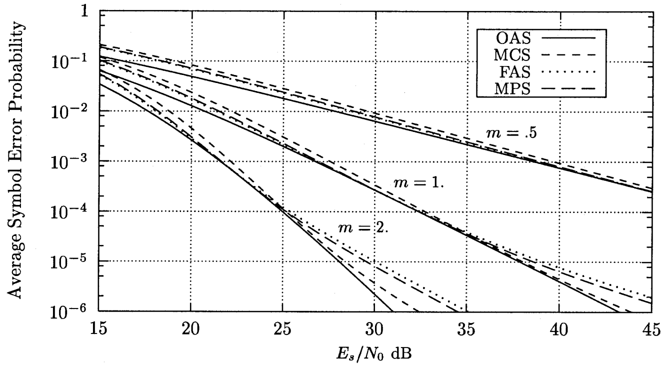


Fig. 10. Average symbol error rate versus $E_s/N_0$ per symbol on each branch for an 8PSK modulation scheme, a normalized distance between antennas $d_a = 0.3$, a normalized Doppler frequency $f_dT_s = 0.03$, and for different values of the fading parameter $m$. Fixed switching thresholds and pilot-to-signal power ratios (Table I) are used. The optimum performance (OAS) of the system is also presented.

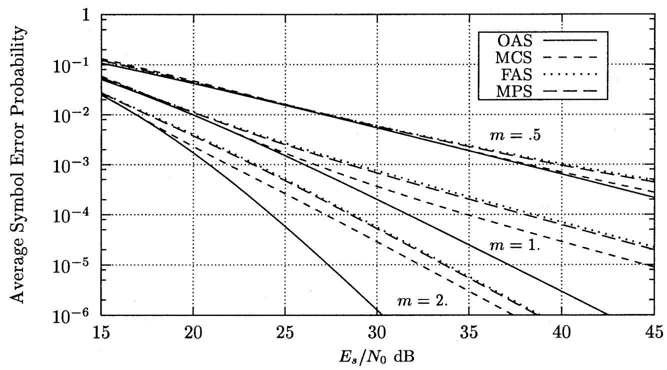


Fig. 11. Average symbol error rate versus $E_s/N_0$ per symbol on each branch for an 8PSK modulation scheme, a normalized distance between antennas $d_a = 0.3$, a normalized Doppler frequency $f_dT_s = 0.01$, and for different values of the fading parameter $m$. Fixed switching thresholds and pilot-to-signal power ratios (Table I) are used. The optimum performance (OAS) of the system is also presented.

and $f_dT_s = 0.03$ is shown. As can be seen from the graph, the average SER performance loss due to the adoption of fixed thresholds is negligible for $m = 0.5$ and is an increasing function of the Nakagami-$m$ fading parameter. In order to analyze the effect of changing the normalized Doppler frequency, Fig. 11 shows the average SER versus $E_s/N_0$ on each branch for $M = 8$, $d_a = 0.3$, $m = 0.5, 1, 2$, and $f_dT_s = 0.01$. The optimization of the fixed switching thresholds and fixed pilot-to-signal power ratios was performed over the range $[f_{d,1}T_s, f_{d,2}T_s] = [0.01, 0.06]$. Thus, comparing the results in Fig. 10, corresponding to a normalized Doppler frequency $f_dT_s = 0.03$ located at the center of the optimization range, with those in Fig. 11, corresponding to a normalized Doppler frequency $f_dT_s = 0.01$ located at the edge of the optimization range, we can conclude that the fixed switching thresholds and fixed pilot-to-signal power ratios are very sensitive to the changes of $f_dT_s$.

## V. Pilot-Symbol-Aided MPSK System

In this case, as shown in (24), a pilot reference symbol is inserted every $(K-1)$ MPSK information symbols within the transmitted data signal sequence. At the receiver, the pilot symbols are filtered by a matched filter and then are fed to an interpolator. As for the PTA system, we will assume that the interpolator takes the form of an equivalent bandpass filter with a bandwidth $B_p = 2f_d$. Thus, assuming a perfect clock recovery, the complex samples at the MPSK detector input at time $t = iT_s$ will be given by

$$w_i = \chi_{\mathrm{ssc}_\tau, i} x_i + n_i \tag{58}$$

$$p_i = \chi_{\mathrm{ssc}_\tau, i} A + \upsilon_i \tag{59}$$

where $n_i$ and $\upsilon_i$ are samples of uncorrelated zero-mean complex Gaussian noise processes with variances $N_0$ and $N_0B_p$, respectively, and it has been assumed, without loss of generality, that $A = B$ and $\theta = 0$ for an MPSK system. Thus

$$\rho_w = \frac{A^2 \left|\chi_{\mathrm{ssc}_\tau, i}\right|^2}{2N_0} = \gamma_{\mathrm{ssc}_\tau} \Rightarrow \alpha_w = \frac{1}{P_w} \tag{60}$$

$$\begin{aligned}\rho_p &= \frac{A^2 \left|\chi_{\mathrm{ssc}_\tau, i}\right|^2}{2N_0 B_p K T_m} = \frac{A^2 \left|\chi_{\mathrm{ssc}_\tau, i}\right|^2}{2N_0 (K-1) B_p T_s} \\ &= \frac{\gamma_{\mathrm{ssc}_\tau}}{(K-1)B_pT_s} \Rightarrow \alpha_p = \frac{1}{(K-1)B_pT_sP_p}.\end{aligned} \tag{61}$$

The average SER $P_s$ can then be written as

$$\begin{aligned}P_s \simeq \frac{M-1}{nM} \sum_{l=1}^{n} & \\ \mathcal{M}_{\gamma_{\mathrm{ssc}_\tau}} & \left[\frac{-\sin^2\left(\frac{\pi}{M}\right)}{(K-1)B_pT_s \sin^2(\kappa_l) + \sin^2\left(\kappa_l + \frac{\pi}{M}\right)}\right].\end{aligned} \tag{62}$$

Under Nakagami-$m$ slow fading conditions, $\gamma_k$ and $\gamma_{k\tau}$ ($k = 1, 2$) can be written as

$$\gamma_k = \frac{A^2|\chi_k|^2}{2N_0(K-1)B_pT_s} \tag{63}$$

$$\gamma_{k\tau} = \frac{A^2|\chi_k|^2}{2N_0} \tag{64}$$

$$\begin{aligned}\overline{\gamma}_k &= \frac{A^2}{2N_0(K-1)B_pT_s} = \frac{r\frac{E_s}{N_0}}{(1+r)B_pT_s} \\ \overline{\gamma}_{k\tau} &= \frac{A^2}{2N_0} = \frac{\frac{E_s}{N_0}}{1+r}\end{aligned} \tag{65}$$

$$\rho_{1,2\tau} = \rho_{2,1\tau} \triangleq \frac{E\{\gamma_1\gamma_{2\tau}\}}{2\sqrt{E\left\{\gamma_1^2\right\} E\left\{\gamma_{2\tau}^2\right\}}} = J_0^2(2\pi d_a) \tag{66}$$

$$\rho_{k,k\tau} \triangleq \frac{E\{\gamma_k\gamma_{k\tau}\}}{2\sqrt{E\left\{\gamma_k^2\right\} E\left\{\gamma_{k\tau}^2\right\}}} = 1 \tag{67}$$

with $E_s = (KA^2/2(K-1))$ and $r = (1/K-1)$ being the equivalent energy per MPSK symbol and the pilot-to-signal power ratio, respectively. Using (65)–(67) in (21) and (62), the expression of $P_s$ reduces after some simplifications to

$$\begin{aligned}P_s \simeq \frac{M-1}{nM} \sum_{l=1}^{n} &\left(1 + \frac{\alpha_l \frac{E_s}{N_0}}{m(1+r)}\right)^{-m} \\ \times &\left[1 + \frac{\Gamma\left(m, \frac{\gamma_T B_p T_s \left[m(1+r) + \alpha_l \frac{E_s}{N_0}\right]}{r\frac{E_s}{N_0}}\right)}{\Gamma(m)} \right. \\ &\left. - \frac{\Gamma\left(m, \frac{m\gamma_T B_p T_s (1+r)\left[m(1+r) + \alpha_l \frac{E_s}{N_0}\right]}{r\left[m(1+r) + \alpha_l\left[1 - J_0^2(2\pi d_a)\right]\frac{E_s}{N_0}\right]\frac{E_s}{N_0}}\right)}{\Gamma(m)}\right]\end{aligned} \tag{68}$$

where

$$\alpha_l \triangleq \frac{\sin^2\left(\frac{\pi}{M}\right)}{\frac{r}{B_pT_s}\sin^2(\kappa_l)+\sin^2\left(\kappa_l+\frac{\pi}{M}\right)}. \tag{69}$$

This expression is identical to that of the PTA system. Thus, as shown by Chan and Bateman in [14], the pilot tone system and the pilot symbol system have the same performance when operating with the same system power and information throughput. The only difference resides in the fact that $r \in \{1/(K-1) : K = 2,3,4,\ldots\}$.

## VI. Differential Detection

In this case, the symbol generated by the digital modulator at time $t = iT_s$, namely, $x_i$, is the phasor representation of the MPSK symbol $\Delta\phi_i$ assigned by the mapper. It can be written as

$$x_i = e^{j\Delta\phi_i}. \tag{70}$$

Before transmission over the channel, the digital modulator output symbol $x_i$ is differentially encoded, producing the encoded symbol $\nu_i$. In phasor notation, the MDPSK coded symbol in the $i$th transmission interval can be expressed as

$$\nu_i = \nu_{i-1}x_i = Ae^{j(\phi_{i-1}+\Delta\phi_i)} = Ae^{j\phi_i} \tag{71}$$

and the baseband equivalent of the transmitted signal is then given by

$$\nu(t) = \sum_i \nu_i q(t-iT_s). \tag{72}$$

Assuming a dual branch diversity system and the use of an ideal automatic frequency control, that is, a perfect compensation of frequency offsets between emitter and receiver local oscillators, the complex envelope of the received signal and the signal at the output of the reception filter can be expressed as

$$r(t) = \chi_{\mathrm{ssc}_\tau}(t)\nu(t) + \mu(t) \tag{73}$$

$$w(t) = \chi_{\mathrm{ssc}_\tau}(t)\sum_i \nu_i h(t-iT_s) + n(t) \tag{74}$$

respectively. In a differential detection receiver, a delayed replica of the input signal, with the time delay $\tau = T_s$, is used as a reference signal (pilot signal). Thus, assuming a perfect clock recovery, the complex samples at the MDPSK detector input at time $t = iT_s$ corresponding to the transmitted symbol $x_i$ will be given by

$$w_i = \chi_{\mathrm{ssc}_\tau,i}\nu_i + n_i \tag{75}$$

$$p_i = w_{i-1} = \chi_{\mathrm{ssc}_\tau,i-1}\nu_{i-1} + n_{i-1}. \tag{76}$$

As in the PTA and PSA receivers, the differential detection process is equivalent to determine the phase angle $\psi$ between the two vectors $w_i$ and $w_{i-1}$ and decide in favor of the symbol $\hat{x}_i$ whose phase is closest to $\psi$. By conditioning on $\chi_{\mathrm{ssc}_\tau,i}$, the complex-valued Gaussian random variable $\chi_{\mathrm{ssc}_\tau,i-1}$ [15], [22], [23] has mean and variance that can be written as

$$\mu_{\chi_{\mathrm{ssc}_\tau,i-1}|\chi_{\mathrm{ssc}_\tau,i}} = J_0(2\pi f_d T_s)\chi_{\mathrm{ssc}_\tau,i} + \left(1-\frac{1}{m}\right)^{\frac{1}{4}}\left[1-J_0(2\pi f_d T_s)\right] \tag{77}$$

$$\sigma^2_{\chi_{\mathrm{ssc}_\tau,i-1}|\chi_{\mathrm{ssc}_\tau,i}} = \frac{\left[1-J_0^2(2\pi f_d T_s)\right]}{2} \tag{78}$$

respectively. Thus, under Nakagami-$m$ slow fading conditions (e.g.,$J_0(2\pi f_d T_s) \simeq 1$) and by conditioning on $\chi_{\mathrm{ssc}_\tau,i}$, the random variables $w_i$ and $w_{i-1}$ are two vectors perturbed by uncorrelated Gaussian noise and

$$\rho_w = \frac{A^2\left|\chi_{\mathrm{ssc}_\tau,i}\right|^2}{2N_0} = \gamma_{\mathrm{ssc}_\tau} \Rightarrow \alpha_w = \frac{1}{P_w} \tag{79}$$

$$\rho_p \simeq \frac{A^2 J_0^2(2\pi f_d T_s)\left|\chi_{\mathrm{ssc}_\tau,i}\right|^2}{2N_0} = J_0^2(2\pi f_d T_s)\gamma_{\mathrm{ssc}_\tau} \Rightarrow \alpha_p = \frac{J_0^2(2\pi f_d T_s)}{P_p}. \tag{80}$$

The average SER $P_s$ can then be approximated as

$$P_s \simeq \frac{M-1}{nM}\sum_{l=1}^{n} \mathcal{M}_{\gamma_{\mathrm{ssc}_\tau}}\left[-\frac{J_0^2(2\pi f_d T_s)\sin^2\left(\frac{\pi}{M}\right)}{\sin^2(\kappa_l)+J_0^2(2\pi f_d T_s)\sin^2\left(\kappa_l+\frac{\pi}{M}\right)}\right]. \tag{81}$$

Obviously, this expression is exact for ideal differential detection, with slow fading. In this case, two consecutive symbols are assumed to fade coherently.

Also, under Nakagami-$m$ slow fading conditions, $\gamma_k$ and $\gamma_{k\tau}$ $(k = 1,2)$ can be written as

$$\gamma_k = \frac{A^2|\chi_k|^2}{2N_0} = \frac{E_s}{N_0}|\chi_k|^2$$

$$\gamma_{k\tau} = \frac{A^2|\chi_{k\tau}|^2}{2N_0} = \frac{E_s}{N_0}|\chi_{k\tau}|^2 \tag{82}$$

with $E_s = A^2/2$ being the equivalent energy per MDPSK symbol. Thus

$$\overline{\gamma}_k = \overline{\gamma}_{k\tau} = \frac{A^2}{2N_0} = \frac{E_s}{N_0} \tag{83}$$

$$\rho_{1,2\tau} = \rho_{2,1\tau} \triangleq \frac{E\{\gamma_1\gamma_{2\tau}\}}{2\sqrt{E\{\gamma_1^2\}E\{\gamma_{2\tau}^2\}}} \simeq J_0^2(2\pi d_a)J_0^2(2\pi f_d T_s) \tag{84}$$

$$\rho_{k,k\tau} \triangleq \frac{E\{\gamma_k\gamma_{k\tau}\}}{2\sqrt{E\{\gamma_k^2\}E\{\gamma_{k\tau}^2\}}} = J_0^2(2\pi f_d T_s) \tag{85}$$

where we have assumed that [4]

$$E\{\chi_1(t)\chi_2^*(t+\tau)\} \simeq J_0(2\pi d_a)J_0(2\pi f_d\tau) \tag{86}$$

$$E\{\chi_k(t)\chi_k^*(t+\tau)\} = J_0(2\pi f_d\tau). \tag{87}$$

In this case, using (82)–(85) in (21) and (81), the expression of $P_s$ reduces after some simplifications to

$$P_s \simeq \frac{M-1}{nM}\sum_{l=1}^{n}\left(1+\frac{\alpha_l\frac{E_s}{N_0}}{m}\right)^{-m} \times\left[1+\frac{\Gamma\left(m,\frac{m\gamma_T\left[m+\alpha_l\frac{E_s}{N_0}\right]}{\left[m+\alpha_l\left[1-J_0^2(2\pi f_d T_s)\right]\frac{E_s}{N_0}\right]\frac{E_s}{N_0}}\right)}{\Gamma(m)} - \frac{\Gamma\left(m,\frac{m\gamma_T\left[m+\alpha_l\frac{E_s}{N_0}\right]}{\left[m+\alpha_l\left[1-J_0^2(2\pi d_a)J_0^2(2\pi f_d T_s)\right]\frac{E_s}{N_0}\right]\frac{E_s}{N_0}}\right)}{\Gamma(m)}\right] \tag{88}$$

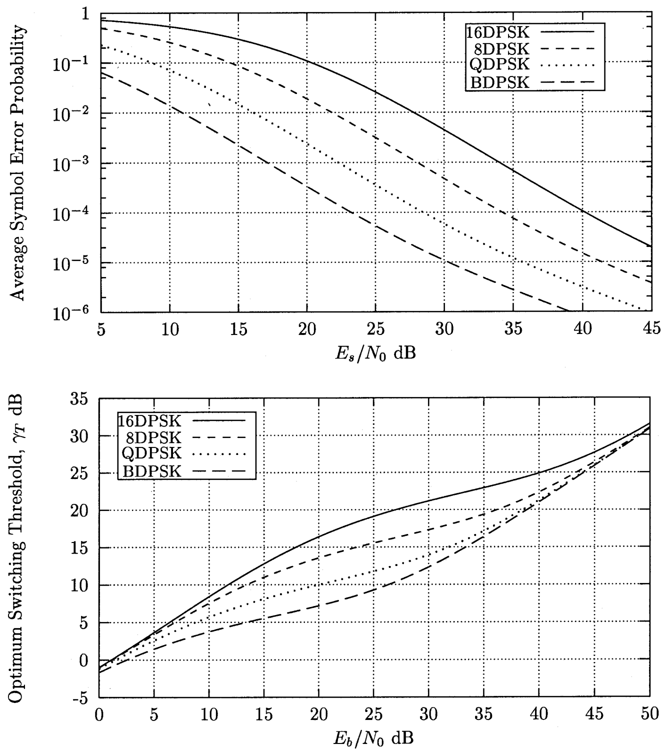


Fig. 12. Optimum performance and optimum switching threshold versus $E_s/N_0$ on each branch for a Nakagami-$m$ fading with $m = 1$ and $f_dT_s = 0.01$, a normalized distance between antennas $d_a = 0.3$, and for different values of alphabet cardinality $M$.

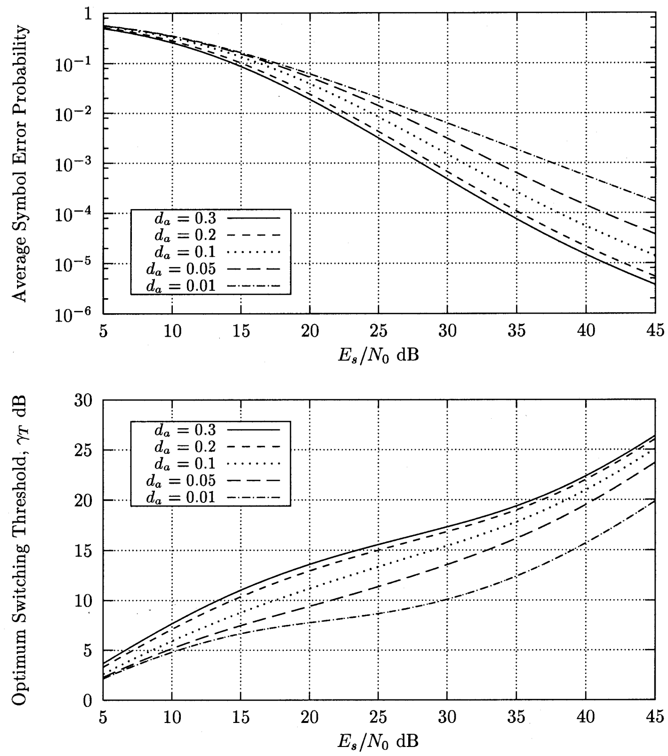


Fig. 13. Optimum performance and optimum switching threshold versus $E_s/N_0$ on each branch for an 8PSK modulation scheme, a Nakagami-$m$ fading with $m = 1$ and $f_dT_s = 0.01$, and for different values of the normalized distance between antennas $d_a$.

where

$$\alpha_l \triangleq \frac{J_0^2(2\pi f_d T_s)\sin^2\left(\frac{\pi}{M}\right)}{\sin^2(\kappa_l) + J_0^2(2\pi f_d T_s)\sin^2\left(\kappa_l + \frac{\pi}{M}\right)}. \quad (89)$$

## A. Optimum Adaptive Performance

The average SER depends not only on $m$, $M$, $E_s/N_0$, $J_0^2(2\pi d_a)$, and $J_0^2(2\pi f_d T_s)$ but also on the value of the switching threshold $\gamma_T$. As the average SER is a continuous function of $\gamma_T$, there exists an optimal value of $\gamma_T$ for which the average SER is minimal. This optimal value $\gamma_T^{\mathrm{OAS}}$ is a solution of

$$\left.\frac{\partial P_s}{\partial \gamma_T}\right|_{\gamma_T = \gamma_T^{\mathrm{OAS}}} = 0. \quad (90)$$

Substituting (36) and (21) into (90) and using [20, 6.5.25], we obtain

$$\int_0^{\frac{(M-1)\pi}{M}} \frac{\frac{1}{b(\varphi)}\exp\left(\frac{-m\gamma_T^{\mathrm{OAS}}\left(\frac{m}{\frac{E_s}{N_0}}+b(\varphi)\right)}{m+b(\varphi)\frac{E_s}{N_0}\left[1-J_0^2(2\pi d_a)J_0^2(2\pi f_d T_s)\right]}\right)}{\left(m+b(\varphi)\frac{E_s}{N_0}\left[1-J_0^2(2\pi d_a)J_0^2(2\pi f_d T_s)\right]\right)^m} d\varphi$$

$$= \int_0^{\frac{(M-1)\pi}{M}} \frac{\exp\left(\frac{-m\gamma_T^{\mathrm{OAS}}\left(\frac{m}{\frac{E_s}{N_0}}+b(\varphi)\right)}{m+b(\varphi)\frac{E_s}{N_0}\left[1-J_0^2(2\pi f_d T_s)\right]}\right)}{b(\varphi)\left(m+b(\varphi)\frac{E_s}{N_0}\left[1-J_0^2(2\pi f_d T_s)\right]\right)^m} d\varphi \quad (91)$$

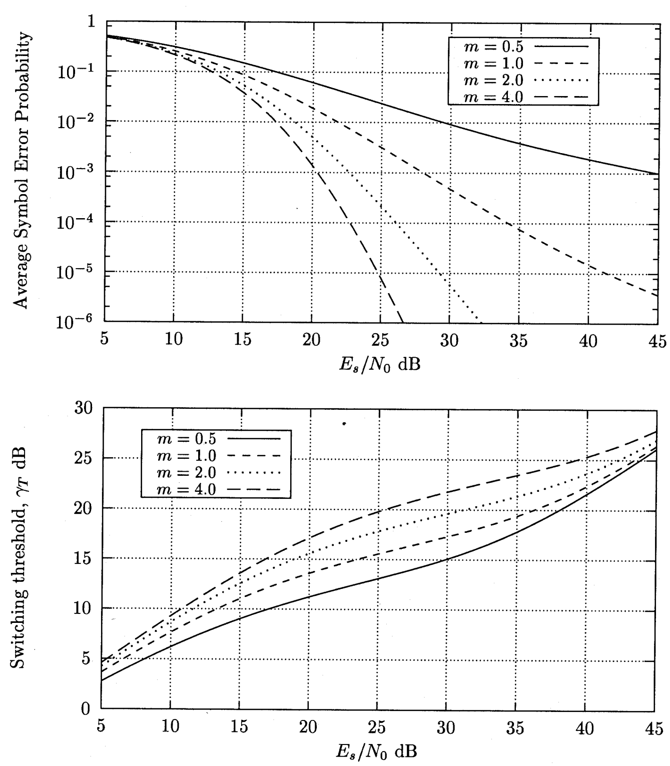


Fig. 14. Optimum performance and optimum switching threshold versus $E_s/N_0$ on each branch for an 8DPSK modulation scheme, a normalized distance between antennas $d_a = 0.3$, and a Nakagami-$m$ fading with $f_dT_s = 0.01$ and different values of $m$.

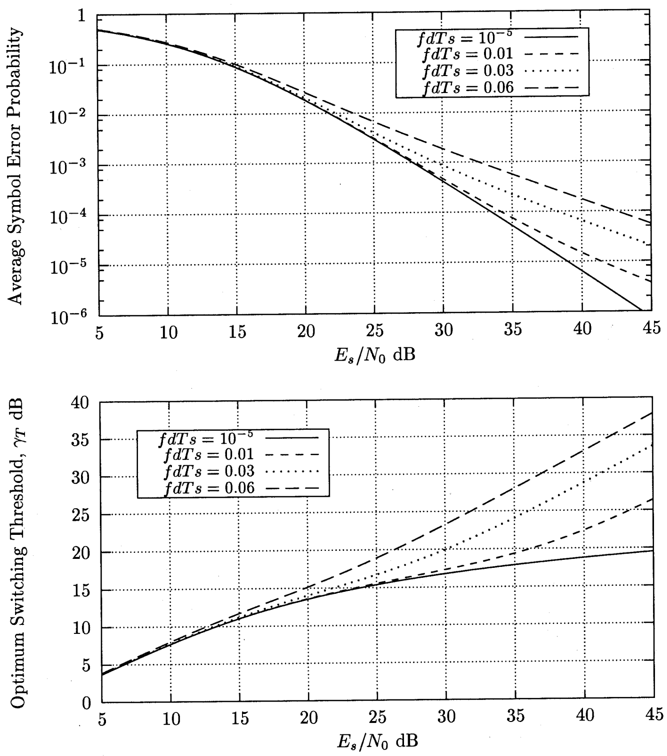


Fig. 15. Optimum performance and optimum switching threshold versus $E_s/N_0$ on each branch for an 8DPSK modulation scheme, a normalized distance between antennas $d_a = 0.3$, and a Nakagami-$m$ fading with $m = 1$ and different values of $f_dT_s$.

where $b(\varphi) = ((J_0^2(2\pi f_dT_s)\sin^2(\pi/M))/(\sin^2\varphi + J_0^2(2\pi f_dT_s)\sin^2(\varphi + \pi/M)))$. Then the optimum switching threshold $\gamma_T^{\rm OAS}$ depends on $m$, $M$, $E_s/N_0$, $d_a$, and $f_dT_s$. In the particular case of BDPSK and very slow fading conditions $(f_dT_s \to 0)$, (91) reduces to

$$\gamma_T^{\rm OAS} = \frac{m\left(m + \frac{E_s}{N_0}\left[1 - J_0^2(2\pi d_a)\right]\right)}{\left[1 - J_0^2(2\pi d_a)\right]\left(m + \frac{E_s}{N_0}\right)} \times \ln\left[1 + \left[1 - J_0^2(2\pi d_a)\right]\frac{E_s}{mN_0}\right] \tag{92}$$

and, for uncorrelated branches, it results that

$$\gamma_T^{\rm OAS} = m\ln\left(1 + \frac{E_s}{mN_0}\right). \tag{93}$$

Figs. 12–15 show the minimum average SER and the optimum switching threshold versus the $E_s/N_0$ on each branch. As expected, the average SER performance is a decreasing function of the symbol alphabet cardinality. Furthermore, for fixed $M$, $m$, and $f_dT_s$, the optimum switching threshold increases with $E_s/N_0$. It is also interesting to point out that, for fixed value of Nakagami-$m$ fading parameter $m$, normalized maximum Doppler shift $f_dT_s$, and normalized distance between antennas $d_a$, the optimum switching threshold is an increasing function of the MPSK alphabet cardinality but becomes rather independent of $M$ for very low and very high values of $E_s/N_0$.

Similarly, as shown in Fig. 13, given a modulation scheme (in this case 8DPSK) and for fixed value of Nakagami-$m$ fading parameter $m$ and normalized maximum Doppler shift $f_dT_s$, the optimum switching threshold is an increasing function of the normalized distance between antennas $d_a$. As $d_a$ tends to zero (totally correlated antennas), the optimum average SER tends to equal that of a single branch receiver. Thus, the results show that, in the range of SER values of practical interest, a diversity gain of several decibels can be obtained for normalized distances between antennas greater than $d_a = 0.05$.

The effect of Nakagami-$m$ fading conditions on the minimum average SER and the optimum switching threshold is analyzed in Figs. 14 and 15. In particular, as expected, the performance improves as $m$ increases, since the fading becomes less severe, and deteriorates as $f_dT_s$ increases, since the correlation between received signal and reference signal decreases. Furthermore, as shown in Fig. 14, given a modulation scheme (in this case 8DPSK) and for fixed value of normalized distance between antennas $d_a$ and normalized maximum Doppler shift $f_dT_s$, the optimum switching threshold is an increasing function of the fading parameter $m$. Also, as shown in Fig. 15, given a modulation scheme (in this case 8DPSK) and for fixed value of normalized distance between antennas $d_a$ and Nakagami-$m$ fading severity $m$, the optimum switching threshold is a decreasing function of the normalized Doppler shift $f_dT_s$.

It is also interesting to consider the sensitivity of the average SER to the value of the switching threshold. To this end, for a fixed average $E_s/N_0 = 20\ dB$ on each branch, Fig. 16 shows the optimum average SER versus switching threshold for different values of alphabet cardinality $M$, normalized distance between antennas $d_a$, and Nakagami fading parameters $m$ and $f_dT_s$. The more the fading parameter $m$ increases, the less sensitive is the average SER to switching threshold variations around the optimum value, independent of the normalized distance between antennas and/or the normalized Doppler frequency of the fading. Moreover, in less severe fading conditions, the sensitivity to $\gamma_T$ increases, especially in slow fading conditions.

### B. Optimum Nonadaptive Performance

Table II shows the values of the fixed thresholds obtained by the application of the proposed strategies (MCS, FAS, and MPS), for different values of alphabet cardinality $M$ and normalized distance between antennas $d_a$. As with pilot-tone-aided systems, the cost function $C(\gamma_T, r)$ has been numerically minimized in order to determine the values of $\gamma_T^{\rm MCS}$. In fact, the triple integral in (40) has been computed numerically over the intervals $[m_1, m_2] = [0.5, 2.0]$, $[f_{d,1}T_s, f_{d,2}T_s] = [0.01, 0.06]$, with $[(E_s/N_0)_1, (E_s/N_0)_2]$ being equal to [15 dB, 35 dB] for BDPSK, [20 dB, 40 dB] for QDPSK, [25 dB, 45 dB] for 8DPSK, and [30 dB, 50 dB] for 16DPSK. The values of $\gamma_T^{\rm FAS}$ have also been obtained through numerical computation of the triple integrals in (41) over the same intervals. Finally, the values of $\gamma_T^{\rm MPS}$ have been obtained using (42) with $\vartheta_{mp} = 1.25$, $\zeta_{mp} = 0.035$, and $\beta_{mp}$ being equal to 25 dB for BDPSK, 30 dB for QDPSK, 35 dB for 8DPSK, and 40 dB for 16DPSK. The results show that for a fixed value of the normalized distance between antennas $d_a$, the fixed switching threshold is an increasing function of the MDPSK alphabet cardinality, independent of the adopted optimum fixed strategy. Furthermore, for a fixed value of $M$, the fixed switching threshold increases with $d_a$.

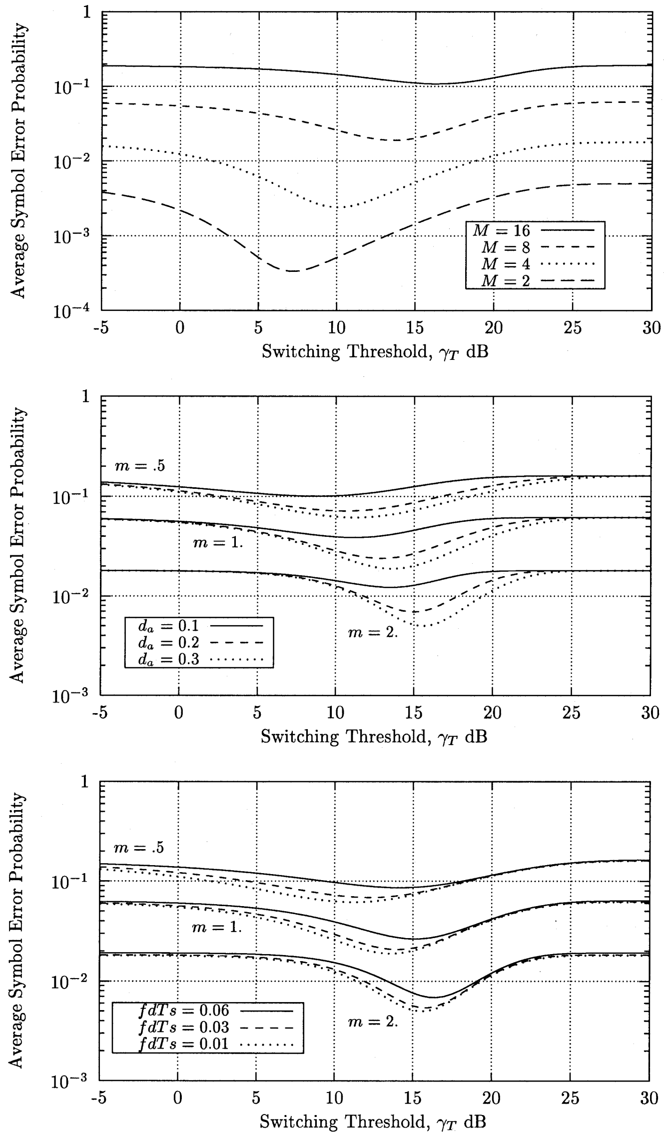


Fig. 16. Average symbol error rate versus switching threshold at a fixed $E_s/N_0 = 20\ dB$ on each branch for different values of alphabet cardinality $M$, normalized distance between antennas $d_a$, and Nakagami fading parameters $m$ and $f_dT_s$. Where not specified, $M = 8$, $d_a = 0.3$, $m = 1$, and $f_dT_s = 0.01$.

With reference to the fixed switching thresholds $\gamma_T^{\mathrm{MCS}}$, $\gamma_T^{\mathrm{FAS}}$, and $\gamma_T^{\mathrm{MPS}}$ of Table II, Fig. 17 shows the average SER versus $E_s/N_0$ on each branch for different values of alphabet cardinality (for clarity, only the SER performance of BDPSK and 16DPSK modulation schemes is presented) and for $m = 1$, $f_dT_s = 0.03$, and $d_a = 0.3$. For comparison purposes, the optimum performance (OAS) of the system is also presented. As can be seen, the SER performances of FAS and MPS are very close to each other and differ with respect to the SER performance of MCS. Similarly, given a modulation scheme (in this case 8PSK) and for fixed value of Nakagami-$m$ fading severity $m = 1$ and normalized maximum Doppler shift $f_dT_s = 0.03$, Fig. 18 shows the average SER versus $E_s/N_0$ on each branch for different values of $d_a$.

The effect of Nakagami-$m$ fading conditions on the average SER is analyzed in Fig. 19, where the average SER versus $E_s/N_0$ on each branch for $M = 8$, $d_a = 0.3$, $m = 0.5, 1, 2,$

TABLE II
FIXED SWITCHING THRESHOLDS FOR BDPSK, QDPSK, 8DPSK, AND 16DPSK WITH $m_1 = 0.5$, $m_2 = 2.0$, $f_{d,1}T_s = 0.01$, AND $f_{d,2}T_s = 0.06$. THE INTERVAL $[(E_s/N_0)_1, (E_s/N_0)_2]$ IS [15 dB, 35 dB] FOR BDPSK, [20 dB, 40 dB] FOR QDPSK, [25 dB, 45 dB] FOR 8DPSK, AND [30 dB, 50 dB] FOR 16DPSK

| $M$ | $d_a$ | $\gamma_T^{MCS}$ | $\gamma_T^{FAS}$ | $\gamma_T^{MPS}$ |
|---|---|---|---|---|
| 2 | 0.1 | 7.4 | 13.2 | 13.1 |
| | 0.2 | 8.9 | 14.3 | 14.5 |
| | 0.3 | 9.5 | 14.8 | 15.0 |
| 4 | 0.1 | 12.0 | 18.2 | 18.0 |
| | 0.2 | 13.8 | 19.2 | 19.5 |
| | 0.3 | 14.3 | 19.7 | 20.0 |
| 8 | 0.1 | 17.2 | 23.5 | 23.1 |
| | 0.2 | 18.4 | 24.3 | 24.5 |
| | 0.3 | 19.4 | 24.8 | 25.0 |
| 16 | 0.1 | 22.3 | 28.9 | 28.2 |
| | 0.2 | 23.7 | 29.3 | 29.6 |
| | 0.3 | 24.7 | 30.1 | 30.1 |

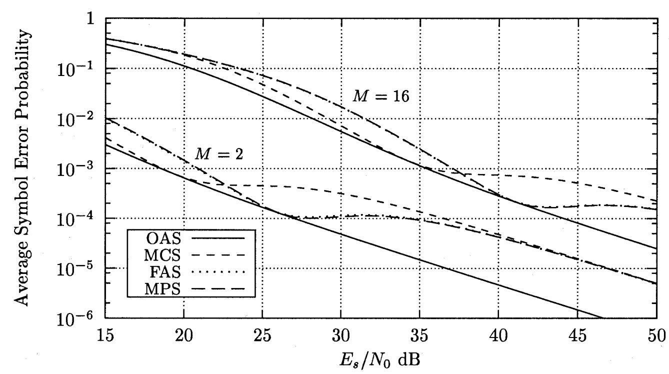


Fig. 17. Average symbol error rate versus $E_s/N_0$ per symbol on each branch for different values of alphabet cardinality $M$ and for $d_a = 0.3$, $m = 1$, and $f_dT_s = 0.03$. Fixed switching thresholds (Table II) are used. The optimum performance (OAS) of the system is also presented.

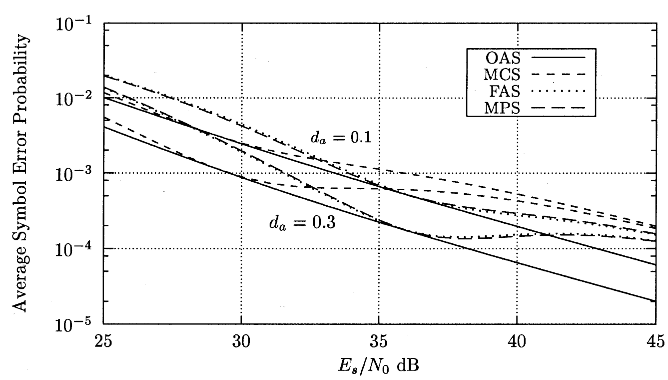


Fig. 18. Average symbol error rate versus $E_s/N_0$ per symbol on each branch for an 8PSK modulation scheme, a Nakagami-$m$ fading channel with $m = 1$ and $f_dT_s = 0.03$, and for different values of normalized distance between antennas $d_a$. Fixed switching thresholds (Table II) are used. The optimum performance (OAS) of the system is also presented.

and $f_dT_s = 0.03$ is shown. As can be seen from the graph, the average SER performance loss due to the adoption of

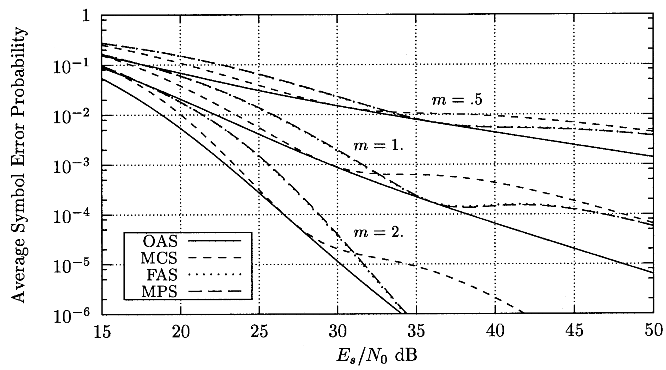


Fig. 19. Average symbol error rate versus $E_s/N_0$ per symbol on each branch for an 8DPSK modulation scheme, a normalized distance between antennas $d_a = 0.3$, a normalized Doppler frequency $f_dT_s = 0.03$, and for different values of the fading parameter $m$. Fixed switching thresholds (Table II) are used. The optimum performance (OAS) of the system is also presented.

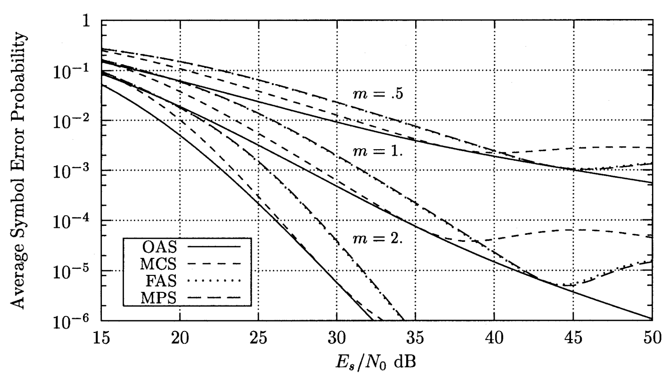


Fig. 20. Average symbol error rate versus $E_s/N_0$ per symbol on each branch for an 8DPSK modulation scheme, a normalized distance between antennas $d_a = 0.3$, a normalized Doppler frequency $f_dT_s = 0.01$, and for different values of the fading parameter $m$. Fixed switching thresholds (Table II) are used. The optimum performance (OAS) of the system is also presented.

fixed thresholds is not negligible even for $m = 0.5$ and is an increasing function of the Nakagami-$m$ fading parameter. In order to analyze the effect of changing the normalized Doppler frequency, Fig. 20 shows the average SER versus $E_s/N_0$ on each branch for $M = 8$, $d_a = 0.3$, $m = 0.5, 1, 2$, and $f_dT_s = 0.01$. The optimization of the fixed switching thresholds and fixed pilot-to-signal power ratios was performed over the range $[f_{d,1}T_s, f_{d,2}T_s] = [0.01, 0.06]$. Thus, comparing the results in Fig. 19, corresponding to a normalized Doppler frequency $f_dT_s = 0.03$ located at the center of the optimization range, with those in Fig. 20, corresponding to a normalized Doppler frequency $f_dT_s = 0.01$ located at the edge of the optimization range, we can conclude that the fixed switching thresholds are rather sensitive to the changes of $f_dT_s$.

Comparing Figs. 8–11 with Figs. 17–20, it can be observed that differential detection with fixed thresholds is more sensitive to $M$, $m$, $d_a$, and $f_dT_s$ than PTA or PSA detection. This sensitivity can be explained by comparing Fig. 6 with Fig. 16. It can be observed that the range of switching thresholds that provide a low average SER is wider for PTA or PSA detection than for differential detection. That is, using a switching threshold different from the optimum is worse for differential detection systems than for PTA or PSA detection systems.

It is worth pointing out that the results presented in this section depend on the selected $m$, $f_dT_s$, and $E_s/N_0$ ranges over which the thresholds are evaluated. Of course, if any of these parameters could be estimated and tracked by the receiver, a certain amount of adaptivity would be achieved.

## VII. Conclusion

The performance of a reference-based dual predetection switch-and-stay diversity system in receiving digitally modulated signals in the presence of additive white Gaussian noise and correlated slow and nonselective Nakagami-$m$ fading channels has been presented. Pilot-tone-aided, pilot-symbol-aided, and differential detection reference-based systems have been considered. The general case of nonideal reference-based channel state information assessment and correlated signal strength fluctuations on the two diversity branches has been investigated. Such a situation can be encountered, for example, in fast fading environments where the diversity antennas are closely spaced, with reference to the RF carrier wavelength, and then receive fast signal fades pertaining to statistical distributions with a certain amount of correlation. The impact of symbol alphabet cardinality, normalized distance between antennas, fading severity, and normalized Doppler frequency on the performance of these systems has been analyzed.

Since the performance of the reference-based switch-and-stay diversity system depends on the switching threshold and on the pilot-to-signal power ratio, the values of these parameters that minimize the average symbol error rate (optimum adaptive strategy) have been obtained. Thus, another goal of this paper has been to determine the optimum switching threshold and the optimum pilot-to-signal power ratio as a function of modulation type, channel fading characteristics, normalized distance between antennas, and average SNR. Furthermore, some fixed switching strategies—minimum cost strategy, fixed average strategy, and midpoint strategy—that allow one to obtain a significant diversity gain with a reduced complexity receiver have been considered.

## References

[1] M. Nakagami, "The $m$-distribution—a general formula of intensity distribution of rapid fading," in *Statistical Methods in Radio Wave Propagation*, W. C. Hoffman, Ed. New York: Elmsford, 1960.

[2] H. Suzuki, "A statistical model for urban multipath propagation," *IEEE Trans. Commun.*, vol. COM-25, Jul 1977.

[3] T. Aulin, "Characteristics of a digital mobile radio channel," *IEEE Trans. Veh. Technol.*, vol. VT-30, May 1981.

[4] W. C. Jakes, Ed., *Microwave Mobile Communications*. New York: Wiley, 1974.

[5] D. G. Brennan, "Linear diversity combining techniques," *Proc. IRE*, pp. 1075–1102, 1959.

[6] D. C. Cox, "Universal digital portable radio communications," *Proc. IEEE*, vol. 75, Apr. 1987.

[7] A. Bateman, "Feedforward transparent tone-in-band: its implementations and applications," *IEEE Trans. Veh. Technol.*, vol. 39, pp. 235–243, Aug. 1990.

[8] S. Sampei and T. Sunaga, "Rayleigh fading compensation method for 16-QAM in digital land mobile radio channels," in *Proc. IEEE 39th Veh. Technol. Conf.*, May 1989.

[9] A. A. Abu-Dayya and N. C. Beaulieu, "Analysis of switched diversity systems on generalized-fading channels," *IEEE Trans. Commun.*, vol. 42, pp. 2959–2966, Nov. 1994.

[10] ——, "Switched diversity on microcellular Ricean channels," *IEEE Trans. Veh. Technol.*, vol. 43, pp. 970–976, Nov. 1994.

[11] G. Femenias and I. Furió, "Analysis of switched diversity TCM-MPSK systems on Nakagami fading channels," *IEEE Trans. Veh. Technol.*, vol. 46, pp. 102–107, Feb. 1997.
[12] G. Fedele, "Switched dual diversity reception of M-ary DPSK signals on Nakagami fading channels," *Wireless Personal Commun.*, vol. 8, pp. 53–71, 1998.
[13] Y.-C. Ko, M.-S. Alouini, and M. K. Simon, "Analysis and optimization of switched diversity systems," *IEEE Trans. Veh. Technol.*, vol. 49, Sept. 2000.
[14] K. Chan and A. Bateman, "The performance of reference-based M-ary PSK with trellis coded modulation in Rayleigh fading," *IEEE Trans. Veh. Technol.*, vol. 41, pp. 190–198, 1992.
[15] A. Papoulis, *Probability, Random Variables, and Stochastic Processes*, 2nd ed. New York: McGraw-Hill, 1984.
[16] A. H. Nuttall, "Some integrals involving the $Q_M$ function," *IEEE Trans. Inform. Theory*, vol. IT-21, Jan. 1975.
[17] I. S. Gradshteyn and I. M. Ryzhik, *Table of Integrals, Series, and Products*, 5th ed. New York: Academic, 1994.
[18] R. F. Pawula, S. O. Rice, and J. H. Roberts, "Distribution of the phase angle between two vectors perturbed by Gaussian noise," *IEEE Trans. Commun.*, vol. COM-30, Aug. 1982.
[19] R. F. Pawula, "Generic error probabilities," *IEEE Trans. Commun.*, vol. 47, May 1999.
[20] *Handbook of Mathematical Functions With Formulas, Graphs, and Mathematical Tables*, Dover, New York, 1964.
[21] A. Annamalai, C. Tellambura, and V. K. Bhargava, "Unified analysis of MPSK and MDPSK with diversity reception in different fading environments," *Electron. Lett.*, vol. 34, no. 16, pp. 1564–1565, Aug. 1998.
[22] W. R. Braun and U. Dersch, "A physical mobile radio channel model," *IEEE Trans. Veh. Technol.*, vol. 40, May 1991.
[23] U. Dersch and R. J. Regg, "Simulation of the time and frequency selective outdoor mobile radio channel," *IEEE Trans. Veh. Technol.*, vol. 42, Aug. 1993.

**Guillem Femenias** (M'91) received the engineer of telecommunication and Ph.D. degrees from the Polytechnic University of Catalonia (UPC), Spain, in 1987 and 1991, respectively.

From 1987 to 1994, he was a Researcher at UPC, where he became an Associate Professor in 1990. Since 1995, he has been an Associate Professor in the Department of Mathematics and Informatics, University of the Balearic Islands, Spain. His current research interests and activities span the fields of digital communications theory with applications and wireless personal communication systems, with particular emphasis on third-generation systems, adaptive modulation techniques, diversity systems, and digital communications over fading channels. He is the author of papers in international journals on these topics as well as of communications for international conferences. He is responsible for several projects concerned with the design of IP-based broadband wireless local-area networks funded by the governments of Spain and the Balearic Islands.